NASA TN D-1011

TECHNICAL NOTE

D-1011

AN INVESTIGATION OF PERIODIC FORCES AND MOMENTS TRANSMITTED TO THE HUB OF FOUR LIFTING ROTOR CONFIGURATIONS

By Milton A. Silveira

Langley Research Center
Langley Air Force Base, Va.

NATIONAL AERONAUTICS AND SPACE ADMINISTRATION

WASHINGTON March 1962

NATIONAL AERONAUTICS AND SPACE ADMINISTRATION

TECHNICAL NOTE D-1011

AN INVESTIGATION OF PERIODIC FORCES AND MOMENTS TRANSMITTED TO THE HUB OF FOUR LIFTING ROTOR CONFIGURATIONS

By Milton A. Silveira

SUMMARY

A wind-tunnel investigation has been conducted to determine the forces and moments transmitted to a rigidly mounted hub of dynamic models of four lifting rotor configurations. The rotor configurations studied included a two-, three-, and four-blade flapping rotor and a two-blade teetering rotor. Variables studied during the investigation included blade collective pitch angles of 0°, 3°, and 6°; rotor angles of attack of -10°, -5°, 0°, and 5°; and combinations of rotational speeds and wind-tunnel velocities which encompassed a range of tip-speed ratio from 0 to 0.45. Most of the data presented is that of the hub thrust loading, with a limited amount of the pitching and torque moments and fore-and-aft force data also being included.

The results of the measurements of the periodic thrust loading reflect the familiar trends of rotor-blade stress measurements; that is, increased periodic forces are measured when the rotor thrust is increased, during transition from hovering to forward flight, and at higher tip-speed ratios. The magnitude of the harmonic forces other than the nth harmonic for an n-blade rotor was generally below 50 percent of the principal (nth) harmonic. The harmonics above the fourth were generally below 20 percent of the principal harmonic force. The principal harmonic of the thrust force was generally found to be below 10 percent of the steady thrust loading at a thrust loading (that is, the thrust coefficient divided by the rotor solidity) above 0.025 and at tip-speed ratios below the point where the periodic thrust loading increases sharply. A comparison of the flapping rotor configurations when operating at the same thrust loading and tip-speed ratio indicates the magnitude of the principal harmonic diminishes materially as the number of blades increases.

The analysis of the limited amount of pitching and torque moments indicates the magnitude of the harmonic components to be about 4 percent and 3 percent, respectively, of the magnitude of the steady components of the moments. The periodic fore-and-aft force, although of the order of magnitude of the steady-force component, was (when omitting the first harmonic component) approximately 5 percent of the steady thrust force.

INTRODUCTION

Limitations have been imposed upon the operation of helicopters and other rotary-wing aircraft as a result of the high vibration levels encountered in flight. The associated high periodic loads imposed on the components, particularly during the so-called transition flight regime, between hovering and forward flight, and during high-speed flight, have contributed substantially to the high rate of replacement and maintenance of component parts.

Efficient design practice for rotary-wing aircraft, which includes appropriate vibration analysis, requires a definition of the loads imposed on the structure as well as an adequate knowledge of the structural characteristics. A method for the determination of the vibration response of helicopters is indicated in reference 1, and procedures for the determination of the natural frequencies of a coupled rotor-fuselage structure are presented in reference 2. The purpose of the present investigation is to evaluate the magnitudes and frequencies of the periodic forces and moments transmitted by the rotor blades to the hub so that the hub supporting structure can be properly designed to minimize the transfer of these forces and moments into the basic rotorcraft structure.

Analytical predictions of the hub loads are difficult, as indicated in reference 3, in that the determination of the loads depends upon an accurate definition of the distribution of induced velocities over the rotor. Since no adequate definition of these velocities is available, a wind-tunnel investigation to measure the loads transmitted to a rigidly mounted hub of several rotor configurations having dynamically scaled rotor blades representative of current full-scale helicopter blades was conducted, and this report presents some of the results obtained. The rotor configurations included a two-, three-, and four-blade flapping rotor and a two-blade teetering rotor. Operating conditions which varied included blade pitch angle, rotor angle of attack, and tip-speed ratio. The results presented in this paper principally cover the periodic components of the axial or thrust force; however, some examples of the periodic components of the fore-and-aft forces and pitching and torque moments are also included.

SYMBOLS

b number of rotor blades

c blade chord, ft

C_T thrust coefficient, $\dfrac{T}{\rho\pi R^2(\Omega R)^2}$

f_n natural frequency of nth elastic mode of blade flapwise bending, cps

H force perpendicular to shaft axis in vertical plane of free-stream velocity, lb

M pitching moment about center of rotor hub, in-lb

Q torque moment about shaft axis, in-lb

L
1
7
2
3

R rotor radius, ft

T thrust force along shaft axis, lb

V free-stream velocity, ft/sec

α rotor angle of attack, deg

ΔC_H harmonic periodic component of H-force coefficient, $\frac{\Delta H}{\rho \pi R^2 (\Omega R)^2}$

ΔC_m harmonic periodic component of pitching-moment coefficient, $\frac{\Delta M}{\rho \pi R^2 (\Omega R)^2 R}$

ΔC_Q harmonic periodic component of torque coefficient, $\frac{\Delta Q}{\rho \pi R^2 (\Omega R)^2 R}$

ΔC_T harmonic periodic component of thrust coefficient, $\frac{\Delta T}{\rho \pi R^2 (\Omega R)^2}$

θ blade collective pitch angle, deg

μ tip-speed ratio, $\frac{V \cos \alpha}{\Omega R}$

ρ air density, slug/cu ft

σ rotor solidity, $bc/\pi R$

Ω rotor speed, radians/sec

APPARATUS AND TESTS

Description of Apparatus

Wind tunnel.- This investigation of the loads on the hubs of dynamic model lifting rotors was conducted in the 17-foot section of the Langley 300-MPH 7- by 10-foot tunnel. The rotor disk, when positioned at a rotor angle of attack of 0°, was located 7.1 feet from the floor of the test section and 8.4 feet from the ceiling. The center of the rotor disk was located 8.0 feet from the test-section walls.

Fuselage and model support.- A fiber-glass fuselage shown in figure 1 was used to cover the dynamic balance (described in the section entitled "Instrumentation") during wind-tunnel testing to reduce airflow interferences caused by the balance. The openings at the rotor shaft and on the bottom of the model were sealed with thin neoprene to prevent flow through the fuselage. The model was mounted to a tripod by a plate hinged at the forward edge which provided a means of varying the rotor and fuselage angle of attack. The rotor angle of attack was positioned by driving tapered pins into holes in two rods located on the rear edge of the hinged plate. The tripod support consisted of three sections of streamline tubing which were bolted to the tunnel floor.

Rotor configurations and blades.- The three- and four-blade fully articulated rotor configurations and the two-blade teetering rotor configuration are shown in figure 1. The details of the flapping rotor are shown in figure 2. A two-blade flapping configuration was obtained by removing, at the flapping hinges, two blades of the four-blade rotor. The rotor diameter was maintained at 66 inches with each configuration. The rotor blades, sketched in figure 3, were uniform in planform and no blade twist was used. The blade profile was the NACA 0015 airfoil with a 2.06-inch chord. The rotor solidity was 0.02 per blade. The mass distribution of the blade and arm is shown in figure 4. The blade chordwise center of gravity was located at 30 percent of the chord. Addition of weights to the rods on the blade-attachment fittings provided a means of eliminating mass unbalance of the rotor due to small irregularities of the blades. The blade Lock number was approximately 8 for the flapping and teetering rotors.

The blade spanwise bending stiffness was such that the flapwise and edgewise bending frequencies are representative of existing full-scale helicopter rotor blades. The average nonrotating-blade flapwise bending frequencies for the flapping rotor were: $f_1 = 6.5$ cps; $f_2 = 21.0$ cps; $f_3 = 47.0$ cps. The average symmetric flapwise bending frequencies for the teetering rotor blade were: $f_1 = 2.6$ cps; $f_2 = 16.5$ cps; and $f_3 = 45.8$ cps. In order to avoid bending-torsion coupling, the blade was

designed to have a high torsional frequency (106.3 cps, average). Frequency variations between blades were less than ±5 percent. The frequency diagram, calculated with the use of reference 4, for the flapping and teetering blades is shown in figure 5.

The flapping rotor configurations were of the fully articulated type, that is, free to flap in the vertical plane and free to lead or lag in the plane of the rotor disk. Blade motion in the plane of rotation was limited to ±12° by positive stops. Small viscous shear-type dampers similar to type F in reference 5 were used to dampen blade motions about the drag hinge. Proper positioning of weights on the rods of the blade-attachment fittings provided a means of making small variations in the angular spacing between blades of the flapping rotors. No built-in cone angle was used on the teetering rotor.

Pitch angles of the blades were adjusted by rotating the blades at the blade-attachment fitting and were locked after the proper pitch angle was set. No provisions were made for cyclic feathering. The pitch axis was located at 25 percent of the blade chord. A small trim tab shown in figure 3 provided a means of making adjustments for proper blade tracking.

The downward flapping of all rotors was limited to 9°. All hinge points on the rotor were journal bearings.

The drive system for the rotor consisted of a small geared air turbine located directly below the hub, which may be considered as having fairly high inertia.

Instrumentation

Balance.- The forces and moments transmitted by the rotor blades to the hub were measured as forces relative to the shaft axis and moments about the center of the rotor as shown in figure 6. The balance specifically designed for this purpose (see fig. 7) used four load cells and two strain-gage beams connected in pairs to measure the load inputs at the rigidly mounted hub. The natural frequencies of all components of the balance were above 100 cps. Two load cells measured the thrust and pitching moment; the other set measured the H-force and torque moment whereas the strain-gage beams sensed the side force and rolling moment. The signals of each pair of transducers were electronically separated into a force and a moment. Interactions between force and moment measuring elements were determined and found to be small and well within the accuracy of the instrumentation. Low-pass filters were employed to remove all frequency inputs above 100 cps. The frequency response of the filter was linear to 95 cps. The rotor speed was indicated by a once-per-revolution contact on the rotor shaft.

Recording equipment.- All signals measured by the balance were simultaneously recorded by an oscillograph recorder and by a tape recorder. The wind-tunnel velocity was read directly from a meter.

Test Procedure

The investigation of the loads on the hubs of lifting rotors was conducted for a number of rotor operating conditions. The hub loads for a two-, three-, and four-blade flapping rotor and a two-blade teetering rotor were measured for blade collective pitch angles of 0°, 3°, and 6°, and rotor angles of attack of -10°, -5°, 0°, and 5° over a range of tip-speed ratios. Wind-tunnel free-stream velocities of approximately 10, 20, 30, 40, 50, and 60 ft/sec were maintained during the tests for a rotor speed of approximately 10 rps. At free-stream velocities of 10, 40, and 60 ft/sec the rotor speed was varied from 7.5 rps to 10.8 rps in increments of 0.415 rps except when prohibited by the flapping motions of the rotor blades or power requirements. The rotor speed was continuously increased from 7.5 rps to 10.8 rps at these three tunnel velocities to determine any areas where an unusual increase in the vibratory levels of the loads occurred and to insure that the intervals of 0.415 rps would be representative samples when the rotor speed is varied.

The steady and periodic loads on the rotor hub were measured by the dynamic balance previously described. The wind-tunnel free-stream velocity was measured by a probe at the height of the rotor and at a position ahead and to the left of the model. The velocity was read for each test condition from a meter. The rotational speed of the rotor was adjusted to the desired value by using a stroboscopic light which also was used to monitor the blade tracking during the run. An air regulation system was used with the driving air turbine which maintained a fairly constant rotor speed when required. The actual rotor speed was obtained from the signal of a once-per-revolution contact on the rotor shaft which was recorded on the oscillograph recorder.

ANALYSIS AND PRESENTATION OF DATA

General Discussion

The periodic components of the forces and moments were determined by two methods: one method consisted of an analog frequency analysis in which the data recorded by the tape recorder was used; the other consisted of a 24-point Fourier analysis of the oscillograph records. Most of the data analyzed was that of the thrust force by using the Fourier analysis. A limited analysis of the H-force and the pitching and torque moments was performed by using the analog frequency analysis.

Due to difficulties encountered in instrumentation during these wind-tunnel tests the side-force and rolling-moment data were not analyzed. No tunnel corrections were applied to the data.

Analog frequency analysis.- The analog frequency analysis is performed by equipment which presents the power spectral density of the levels of the various frequency components by analyzing a continuous loop of the data recorded on the magnetic tape. The tape loop consists of a 30-second sample of a steady operating condition. It was analyzed by use of a filter having a width of 1 cps sweeping from 0 to 100 cps. The levels of all nonperiodic forces with frequencies between 0 and 100 cps are obtained in addition to the forces which have frequencies which are harmonics of the rotor speed.

Fourier analysis.- The Fourier analysis was performed by analyzing a specified number of values of the data (as recorded on the oscillograph record) which are obtained at evenly divided intervals within one revolution. It was determined that a 24-point analysis (reading 24 values per revolution) would adequately define the first eight harmonics of all the rotor speeds used. When the data were analyzed by use of the Fourier analysis, at least three revolutions were sampled for each steady-state condition. The three revolutions selected were the smoothest, roughest, and one condition between these two vibration levels measured when these variations existed during the wind-tunnel test. The values from the Fourier analysis presented are the average values of the three revolutions analyzed. At high vibration levels the differences between the values of the three cycles were of the order of ±15 percent. A digital computer was used to perform the numerical computations.

Presentation of Data

A few representative analyses of the thrust loading showing the relative order of magnitude of the various harmonic components up to the eighth harmonic are shown for the two-, three-, and four-blade flapping rotors and the two-blade teetering rotor in figures 8 to 11. The harmonic components of the thrust loading are normalized on the level of the principal harmonic, that is, the nth harmonic of an n-blade rotor. The principal harmonic and multiples of the principal harmonic are shown as the hatched bars. These are the harmonics not expected to cancel at the rotor hub.

In order to further define the rotor operating condition, the steady thrust loading coefficient C_T/σ (the thrust coefficient divided by the rotor solidity) for blade pitch angles of 0°, 3°, and 6° is shown plotted against tip-speed ratio for various rotor angles of attack in the upper portions of figures 12, 13, and 14. The thrust loading coefficient was measured at several rotor speeds as indicated by the symbols in the figures.

The magnitudes of the principal periodic components of the thrust loading coefficient $\Delta C_T/\sigma$ (where ΔC_T in this case is defined as the amplitude of the nth harmonic of the periodic thrust expressed in the form of the thrust coefficient) of some of the steady thrust loading shown in the upper portions of figures 12, 13, and 14 are plotted against tip-speed ratio in the lower portions of the figures. The principal harmonic of the thrust force presented in these figures was obtained by using the Fourier analysis. Some initial values were obtained by using the analog frequency analysis to determine if any noise or extraneous frequencies were being measured. After it was determined that the thrust periodic components were those of the harmonics of the rotor speed, the more rapid Fourier analysis was used. The values of the periodic thrust loading coefficient shown in figures 12, 13, and 14 are those determined for a rotor speed of approximately 10 rps as indicated by the symbols on the curves for the four rotor angles of attack. Figure 15 shows some curves of the periodic thrust loading coefficient presented in figures 12, 13, and 14 with additional data points shown for values obtained at rotor speeds other than 10 rps.

The principal harmonic of the periodic thrust loading coefficient for the various rotor configurations is compared when applicable in figure 16. These comparisons of $\Delta C_T/\sigma$ are limited to those conditions when the rotor angle of attack and blade pitch angle are the same and when the values of C_T/σ presented in figures 12, 13, and 14 are nearly the same. These results are a cross plot of the values first presented in figures 12, 13, and 14.

A limited amount of data showing the variations of the periodic components of the pitching moment, the H-force, and the torque moment is presented in figures 17, 18, and 19. These values were derived by using the analog frequency analysis and are presented to indicate the trend of forces and moments measured during five rotor operating conditions for which the principal harmonic of the periodic thrust loading has previously been shown.

DISCUSSION OF RESULTS

Analyses of the harmonic loads of the thrust measured on the rotor hub and shown in figures 8 to 11 reflect the large magnitude of the principal harmonic as compared with the harmonic components of other orders. Although some relatively large first-harmonic forces which may be due to a blade out of track were measured on the four-blade flapping rotor, the magnitude of most of the other harmonic components is below half the value of the principal harmonic. Harmonic components above the fourth are generally below 20 percent of the value of the principal

harmonic. In view of this fact, most of the data presented in this paper is that of the principal harmonic of the thrust loading.

Although fixing the rotor angle of attack, blade pitch angle, rotor speed, and forward velocity (wind-tunnel velocity) does not provide exactly the same flow condition for the different number of blades, the variation in the vibration levels obtained during this investigation has been presented for particular rotor angles of attack and blade pitch angles and is plotted against tip-speed ratio as a convenient method of presenting the data. It should be noted in plotting against tip-speed ratio that although this parameter is the basic one in the region of high forward velocity, such is not the case in the region of low forward velocity where induced flow variations have the primary effect.

The thrust loading coefficient was measured at several rotor speeds and wind-tunnel velocities as indicated in the upper portions of figures 12, 13, and 14. Although there is some scatter, the trends for the four angles of attack are generally well defined. It should be noted that values of the thrust loading coefficient C_T/σ for the condition of hovering vary more than expected by changing the rotor solidity of each rotor configuration when the same pitch angle is considered. This variance is due to the difficulties encountered in setting the pitch angles of small blades and the additional problem of obtaining good blade tracking. The variations of the hovering thrust loading for the same rotor configuration and the same pitch angle but for different rotor angles of attack are due to small variations in the rotor speed. The values of the rotor speed indicated by the symbols are the prescribed values used during the wind-tunnel investigation. The actual rotor speed as obtained from the once-per-revolution indicator, which was used to determine the coefficients and tip-speed ratio, may vary up to 5 percent of the prescribed value. In the case of the four-blade flapping rotor at $\theta = 6^\circ$ (fig. 14(c)) the hovering thrust loading could not be obtained at 10 rps because of the power limitation of the air turbine.

The periodic thrust loading coefficients $\Delta C_T/\sigma$ plotted in the lower portions of figures 12, 13, and 14 show the variation of the periodic thrust with tip-speed ratio for a rotor speed of approximately 10 rps. The vibration levels for a collective pitch angle of 0° indicate a similarity in trends of the principal harmonic for the four rotor angles of attack when plotted against tip-speed ratio. (See fig. 12.) When the rotors are operating at an absolute value of C_T/σ of 0.025 or greater, the principal harmonic is generally below 10 percent of the steady thrust force up to a tip-speed ratio of 0.25 where the vibration level starts to increase sharply to values greater than 20 percent of the steady thrust force. At the higher tip-speed ratios, the largest values of the vibration levels, when each configuration is considered

separately, were measured where the absolute value of the thrust loading coefficient is greatest. This trend is also generally true for the collective pitch angles of 3° and 6° as shown in figures 13 and 14. The increase in vibration level with thrust loading coefficient in the range of tip-speed ratios of this investigation indicates a dependence upon the thrust loading of the rotor presumably resulting from the increasing complexity of the variations in blade angle of attack, including in some instances retreating blade stall as well as the reversed velocity region.

An examination of figures 13 and 14 also indicates that the periodic thrust loading coefficient increases as the rotor moves from the hovering flight condition into the transition flight region then decreases somewhat as the forward flight velocity was increased before the coefficient increased again at the high forward flight velocities. This trend in the transition flight region is probably due to the magnitude of flow asymmetry associated with the transition flight region of rotor aircraft and is similar to the high rotor-blade bending loads measured in this region during previous investigations. Consequently, this first peak of the periodic thrust loading coefficient occurs at different values of the tip-speed ratio for different thrust coefficients. The magnitude of the principal harmonic shown in figures 13 and 14 is generally below 10 percent of the steady thrust when C_T/σ is greater than 0.025 and at tip-speed ratios below the point where the sharp increase in the principal harmonic occurs. At the higher tip-speed ratios, the magnitude of the principal harmonic in some cases exceeded 40 percent of the steady thrust coefficient before the testing was terminated.

L 1 7 2 3

The variation of the principal harmonic with tip-speed ratio is shown again for some rotor operating conditions in figure 15 with additional measured values which were obtained at several rotor speeds. In general, the agreement of the periodic thrust loading coefficients over a range of rotor speeds with those obtained at 10 rps was probably due to the limited variations in rotor-blade resonant condition when the rotor speed is varied.

Figure 16 shows a comparison of the vibration levels based on comparable values of C_T/σ and tip-speed ratio of the rotor configurations. The principal harmonic for each configuration is shown for the same rotor angle of attack and blade pitch angle and where the values of C_T/σ are nearly the same. These data are selected from figures 12, 13, and 14. The comparison of the rotor configuration generally indicates that the vibratory levels of the two-blade and the three-blade flapping rotor are greater than those of the four-blade flapping rotor. It will be recalled that for identical blades the inputs for harmonic orders less than the number of blades are expected to cancel. The reduced vibration levels of the rotors with increasing number of blades may be attributed to the sharply reduced magnitude of the aerodynamic forces with

increase in harmonic order. These reduced magnitudes are well illustrated by the trends shown in figures 8 to 11. In the only comparison of the two-blade flapping and two-blade teetering rotor (fig. 16(i)) the flapping-blade vibration level is in some cases twice that of the teetering rotor.

The analysis of some of the vibration levels of the pitching moment is shown in figure 17. These levels are rather small in that the vibratory levels are about 4 percent of the small steady pitching moment. However, the variations of the levels with tip-speed ratio are shown in the figure and represent the harmonics of the rotor speed which were large enough to be measured by the analog frequency analysis. The harmonic loads for the four-blade rotor shown in figures 17(a) to 17(d) indicate harmonics of the first, second, and fourth order. Some third-harmonic pitching moment also appears in the analysis. For the three-blade rotor (fig. 17(e)) the harmonic loads were the first, second, and third.

A limited analysis was also performed of the vibration levels of the H-force, or in this case the aft force, for the same test conditions and rotors and is presented in figure 18. The amplitude of the periodic fore-and-aft force is presented in the form of the force coefficient divided by the solidity and was determined by using the analog frequency analysis. The fact that the rotor configuration did not use cyclic feathering should be kept in mind in examining these results. Although the periodic fore-and-aft force measured is of the same order of magnitude as the steady fore-and-aft force because the steady force is small, the periodic forces other than the first harmonic are a maximum of 5 percent of the steady thrust force. The analysis indicates the first, second, and fourth harmonic forces for the tests involving the four-blade rotor. The vibratory levels of the H-force of the three-blade rotor consisted mainly of a first and second harmonic and are considerably lower than those for the four-blade rotor.

Variations of the periodic torque moment for the identical tests presented in figures 17 and 18 and for these specific rotor configurations are shown in figure 19. As for the H-force the absence of cyclic feathering on the rotor configuration should again be kept in mind. The periodic torque moments are generally below 3 percent of the steady torque value. The harmonics for the four-blade rotor indicate harmonics of the torque moment up to the fifth order. For the three-blade rotor the second and third harmonics are predominant with some first and fourth harmonics indicated.

CONCLUDING REMARKS

A wind-tunnel investigation has been conducted to measure the forces and moments transmitted to the rotor hub of dynamic models of four

lifting rotor configurations during a number of operating conditions. The results of the measurements of the periodic thrust loading at the rotor hub reflect the familiar trends of rotor-blade stress measurements; that is, increased periodic forces are measured when the rotor thrust is increased, during transition from hovering to forward flight, and at higher tip-speed ratios. The magnitude of the principal-harmonic loading of the thrust, that is, the nth harmonic for an n-blade rotor, was generally twice that of any of the other harmonics. The magnitude of the harmonic loading above the fourth harmonic was generally below 20 percent of that of the principal harmonic. The variation of the principal-harmonic thrust loading with tip-speed ratio indicates that the levels are generally below 10 percent of the steady thrust loading when the rotor is operating at a thrust loading (thrust coefficient divided by rotor solidity) greater than 0.025 and at tip-speed ratios below where the principal-harmonic loading increases sharply. A comparison of the principal-harmonic thrust loading for the flapping rotors indicates that the principal harmonic of the two-blade rotor is greater than that of the three-blade rotor which in turn is greater than that of the four-blade rotor when the rotor blades are operated at the same thrust loading.

L 1 7 2 3

Although the analysis of the pitch and torque moments and the fore-and-aft force was limited, some general remarks for these specific rotor configurations may be made. The harmonic components of the pitching moment and torque moment measured were small when compared with the steady components, being 4 percent and 3 percent, respectively, of the magnitude of the steady moments. The harmonic components of the fore-and-aft force were found to be of the same order of magnitude of the steady aft force, but for harmonics other than the first, the values are approximately 5 percent of the steady thrust force.

Langley Research Center,
National Aeronautics and Space Administration,
Langley Air Force Base, Va., October 26, 1961.

REFERENCES

1. Yeates, John E., Jr., Brooks, George W., and Houbolt, John C.: Flight and Analytical Methods for Determining the Coupled Vibration Response of Tandem Helicopter. NACA Rep. 1326, 1957. (Supersedes NACA TN 3852 by Yeates and TN 3849 by Brooks and Houbolt.)

2. Silveira, Milton A., and Brooks, George W.: Analytical and Experimental Determination of the Coupled Natural Frequencies and Mode Shapes of a Dynamic Model of a Single-Rotor Helicopter. NASA MEMO 11-5-58L, 1958.

3. Ham, Norman D., and Zvara, John: Experimental and Theoretical Analysis of Helicopter Rotor Hub Vibratory Forces. WADC Tech Rep. 59-522, U.S. Air Force, Oct. 1959.

4. Yntema, Robert T.: Simplified Procedures and Charts for the Rapid Estimation of Bending Frequencies of Rotating Beams. NACA TN 3459, 1955. (Supersedes NACA RM L54G02.)

5. Silveira, Milton A., Maglieri, Domenic J., and Brooks, George W.: Results of an Experimental Investigation of Small Viscous Dampers. NACA TN 4257, 1958.

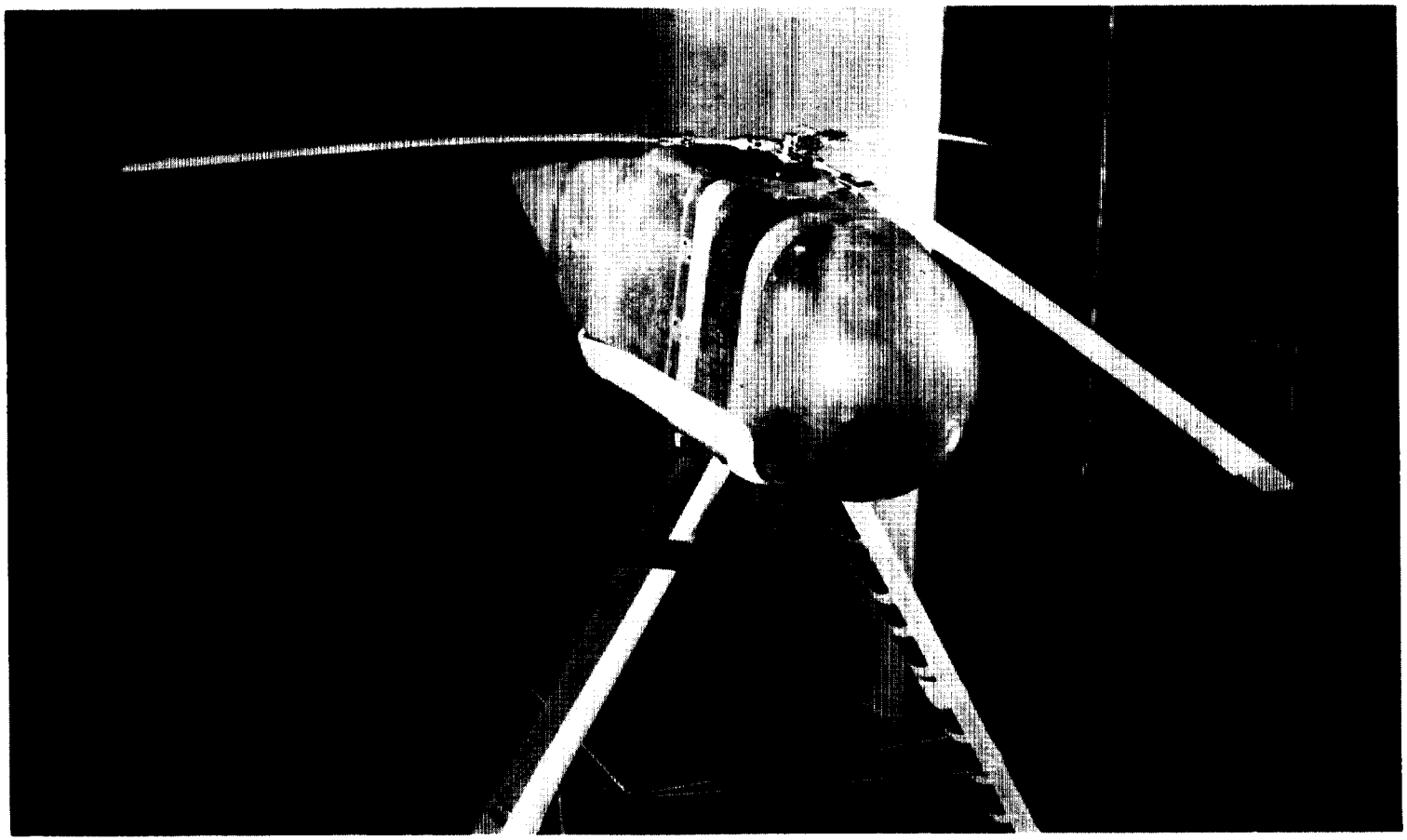

(a) Three-blade flapping rotor. L-59-3786

Figure 1.- Model rotor configuration.

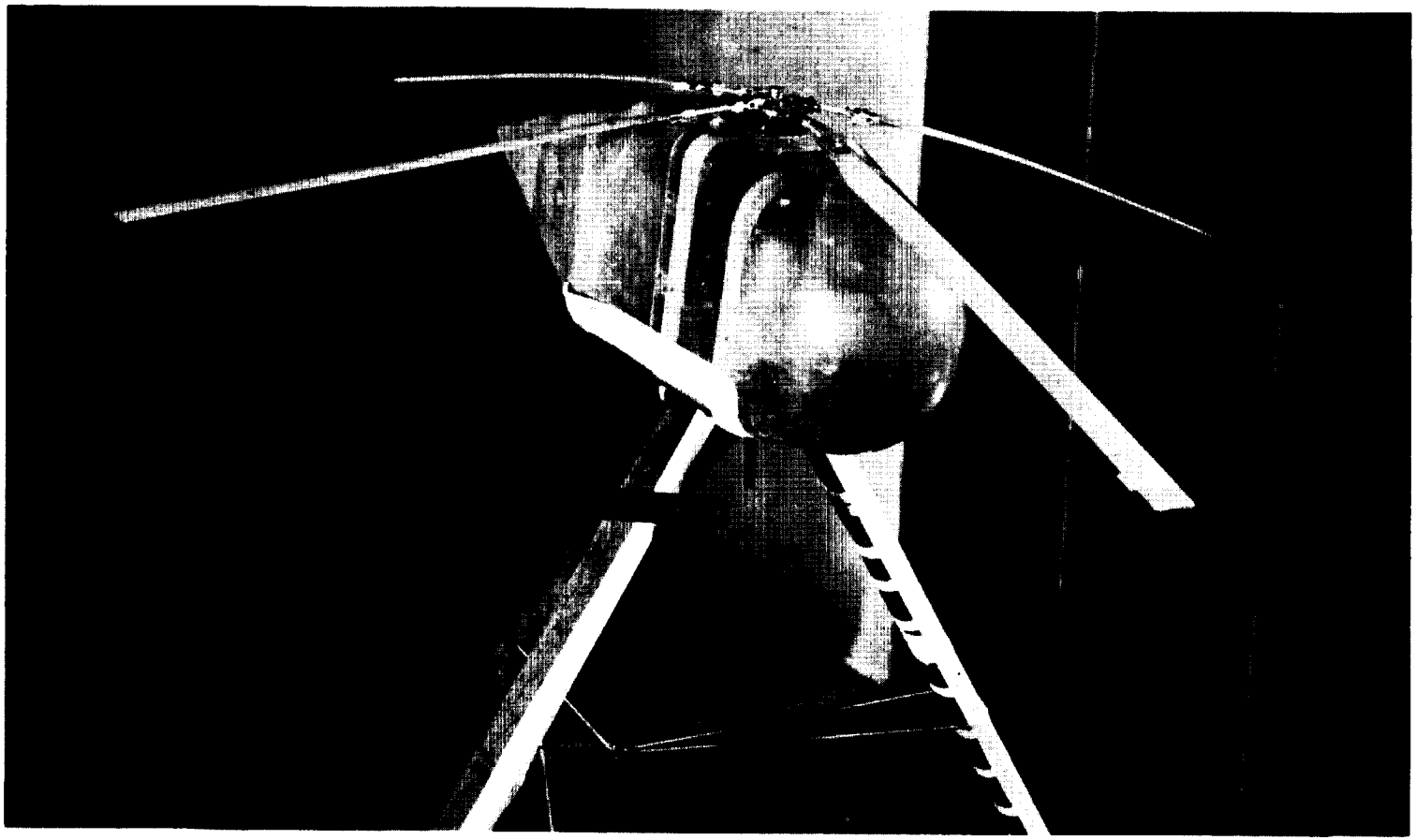

(b) Four-blade flapping rotor. L-59-3787

Figure 1.- Continued.

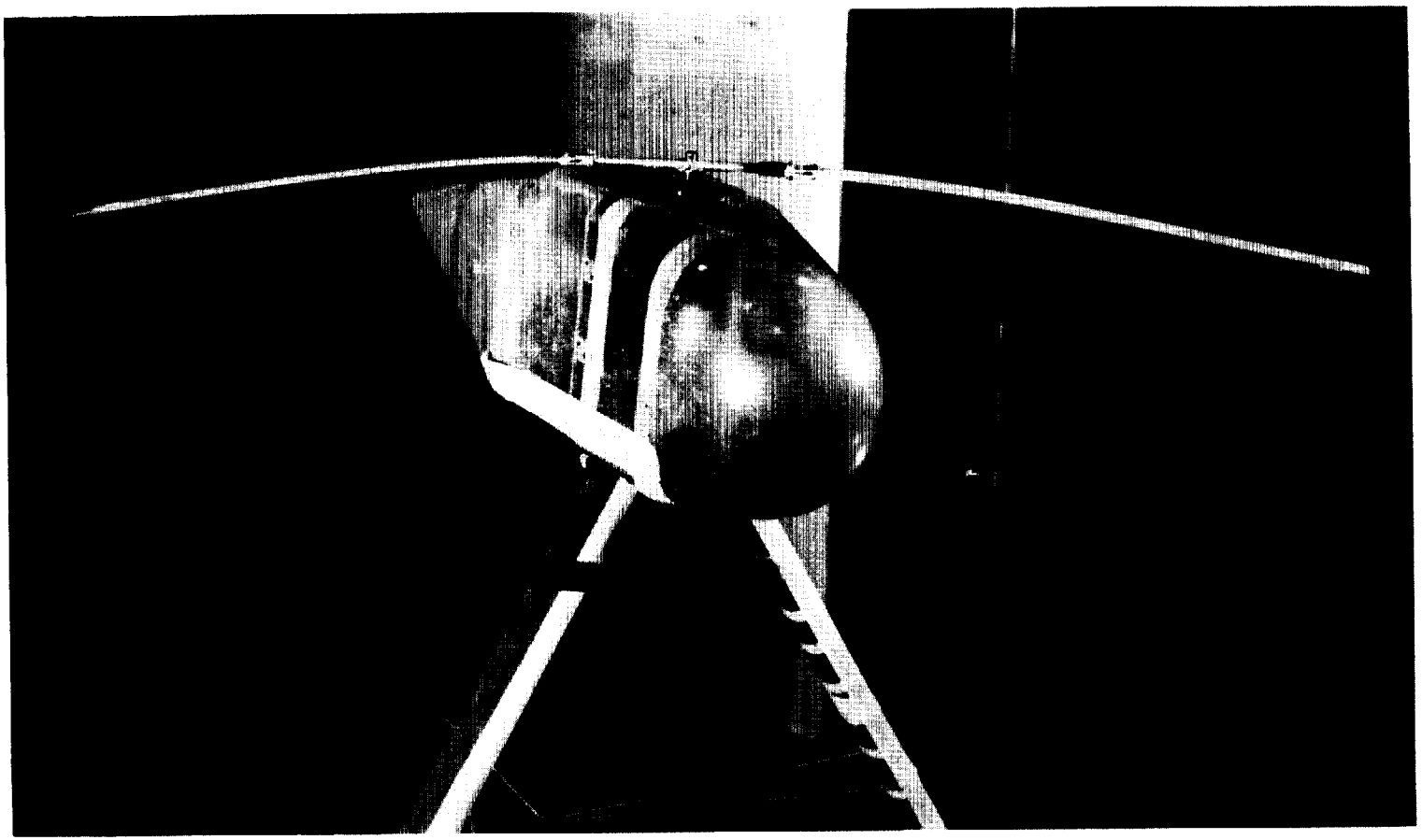

(c) Two-blade teetering rotor. L-59-3788

Figure 1.- Concluded.

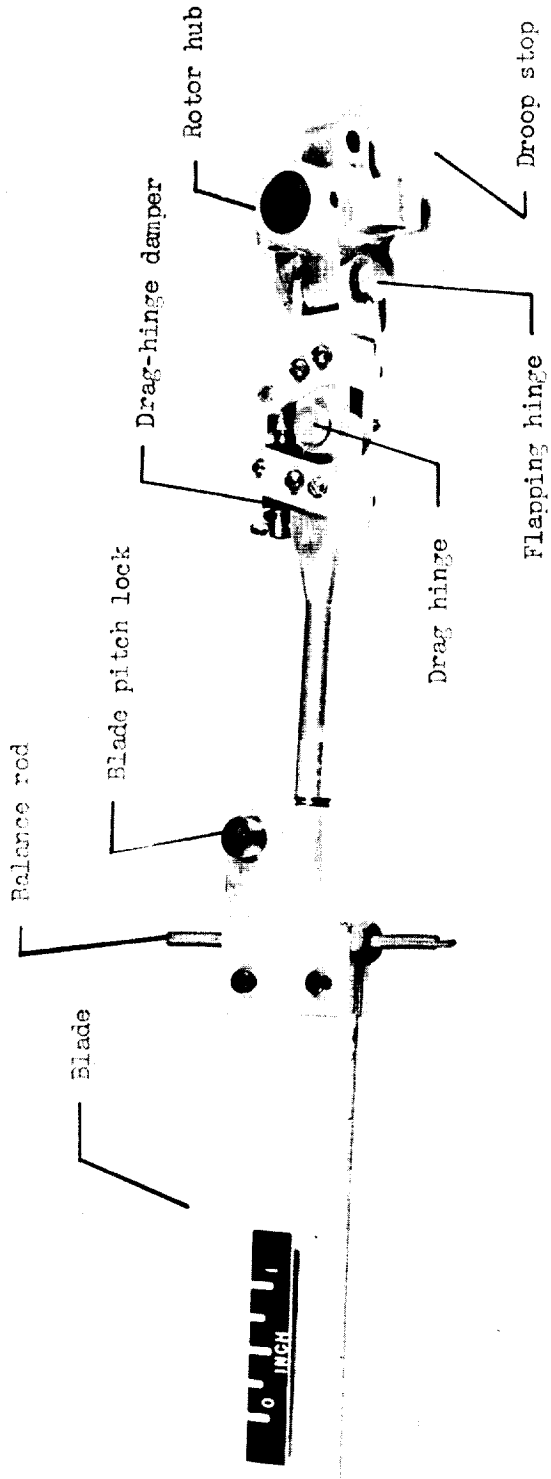

Figure 2.- Rotor-blade arm assembly.

L-61-3210.1

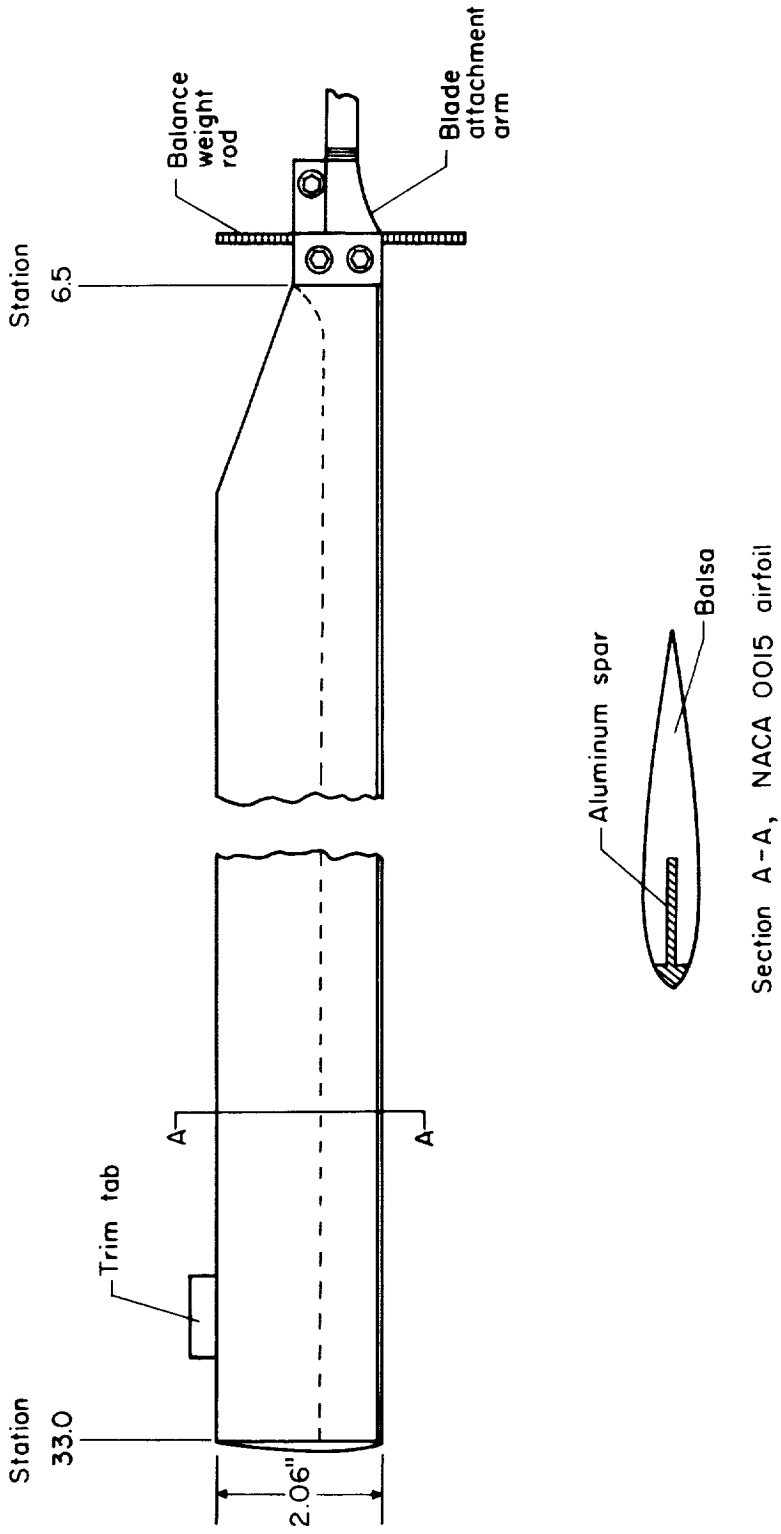

Section A-A, NACA 0015 airfoil

Figure 3.- Rotor blade.

L-1167

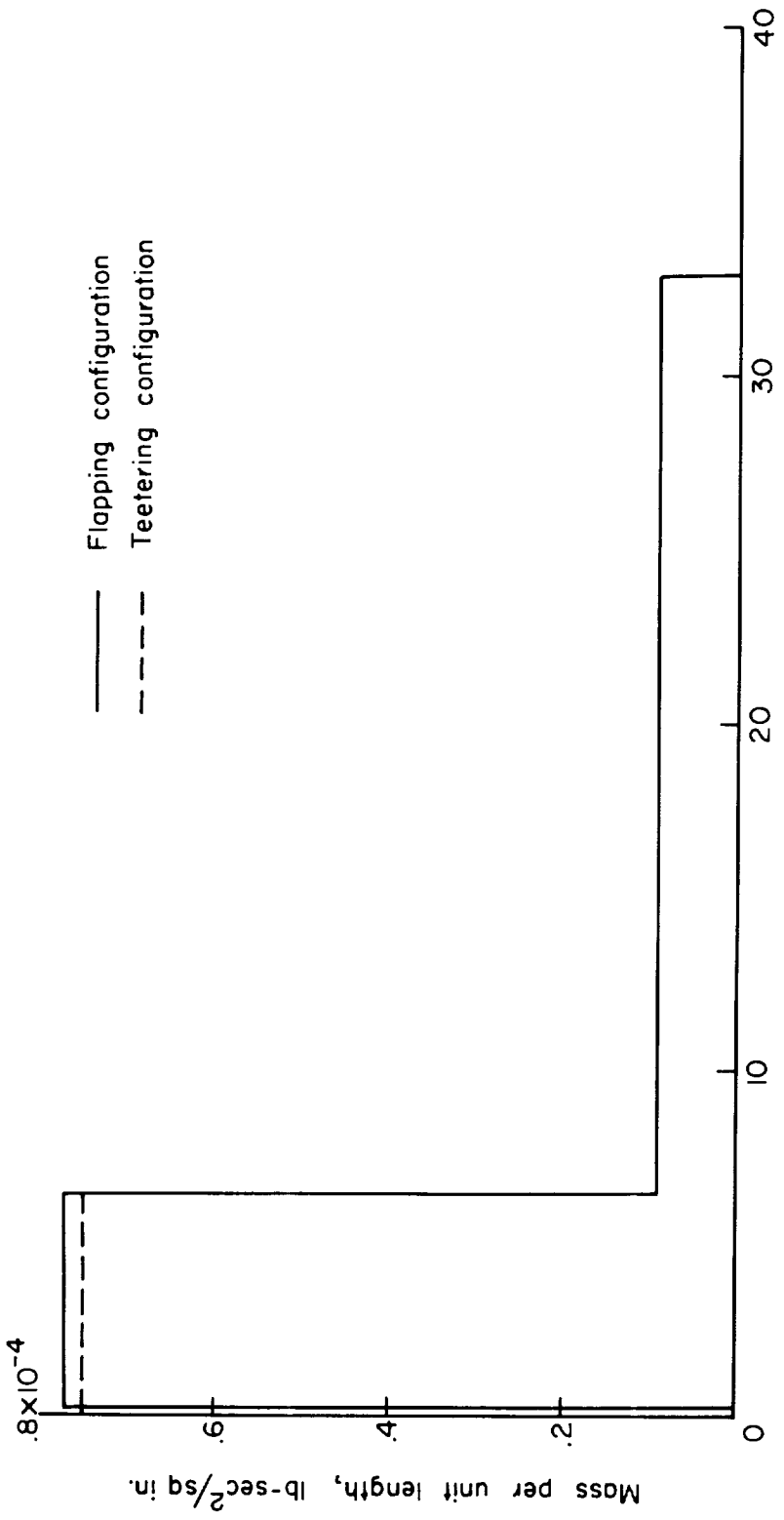

Figure 4.- Blade mass distribution.

L-1723

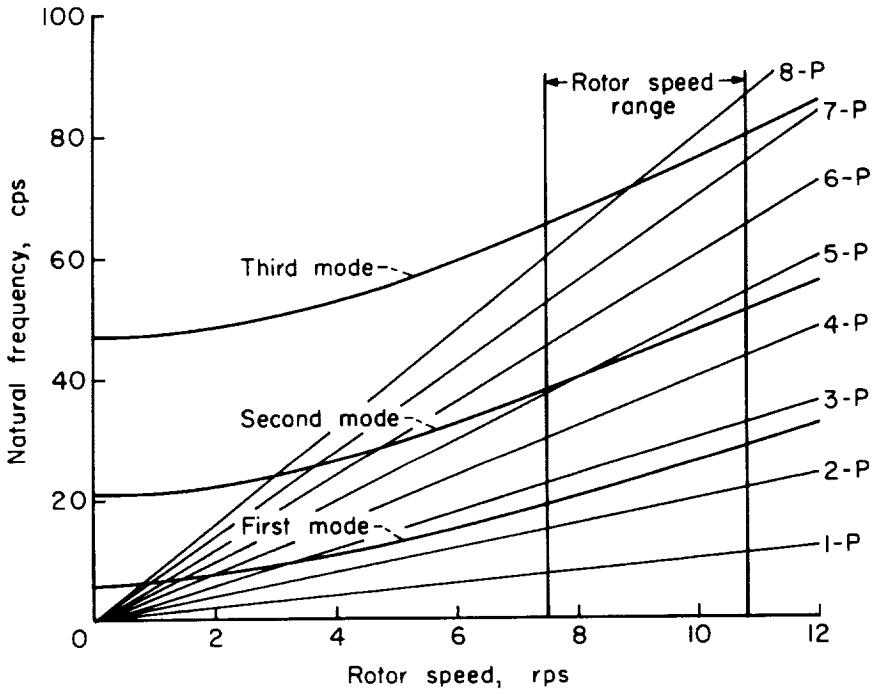

(a) Flapping rotor.

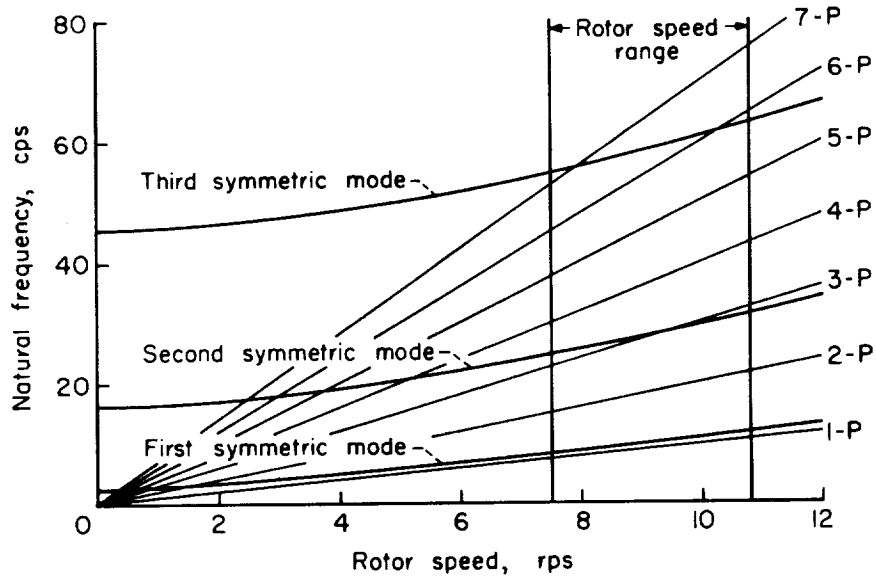

(b) Teetering rotor.

Figure 5.- Frequency diagram.

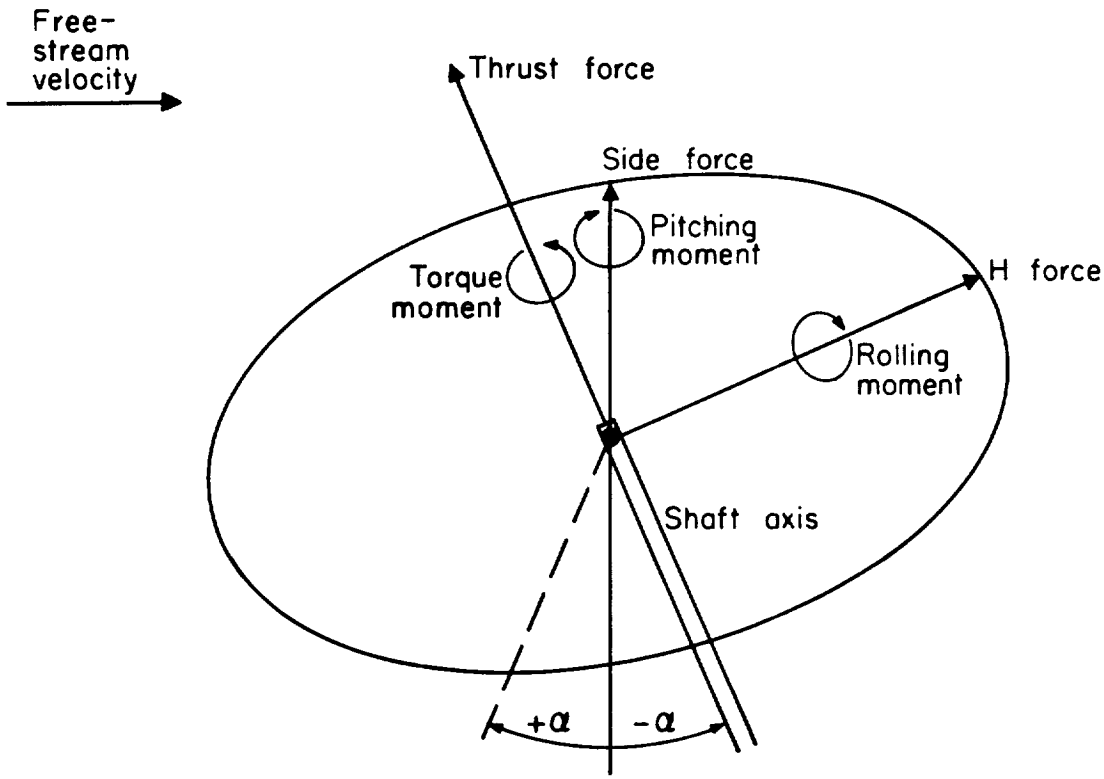

Figure 6.- Identification of forces and moments. (Directions shown are positive.)

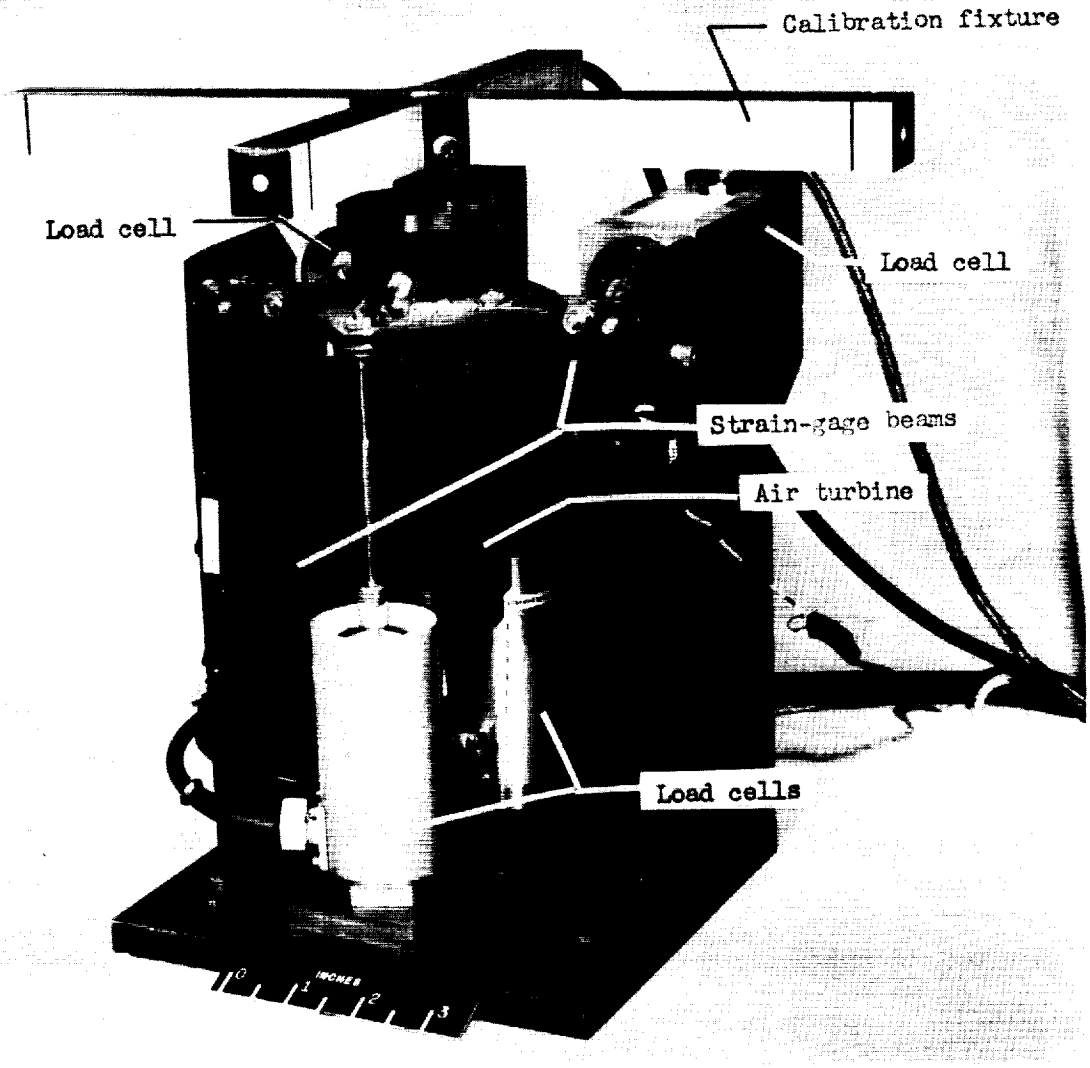

(a) Front view. L-58-1168.1

Figure 7.- Dynamic balance.

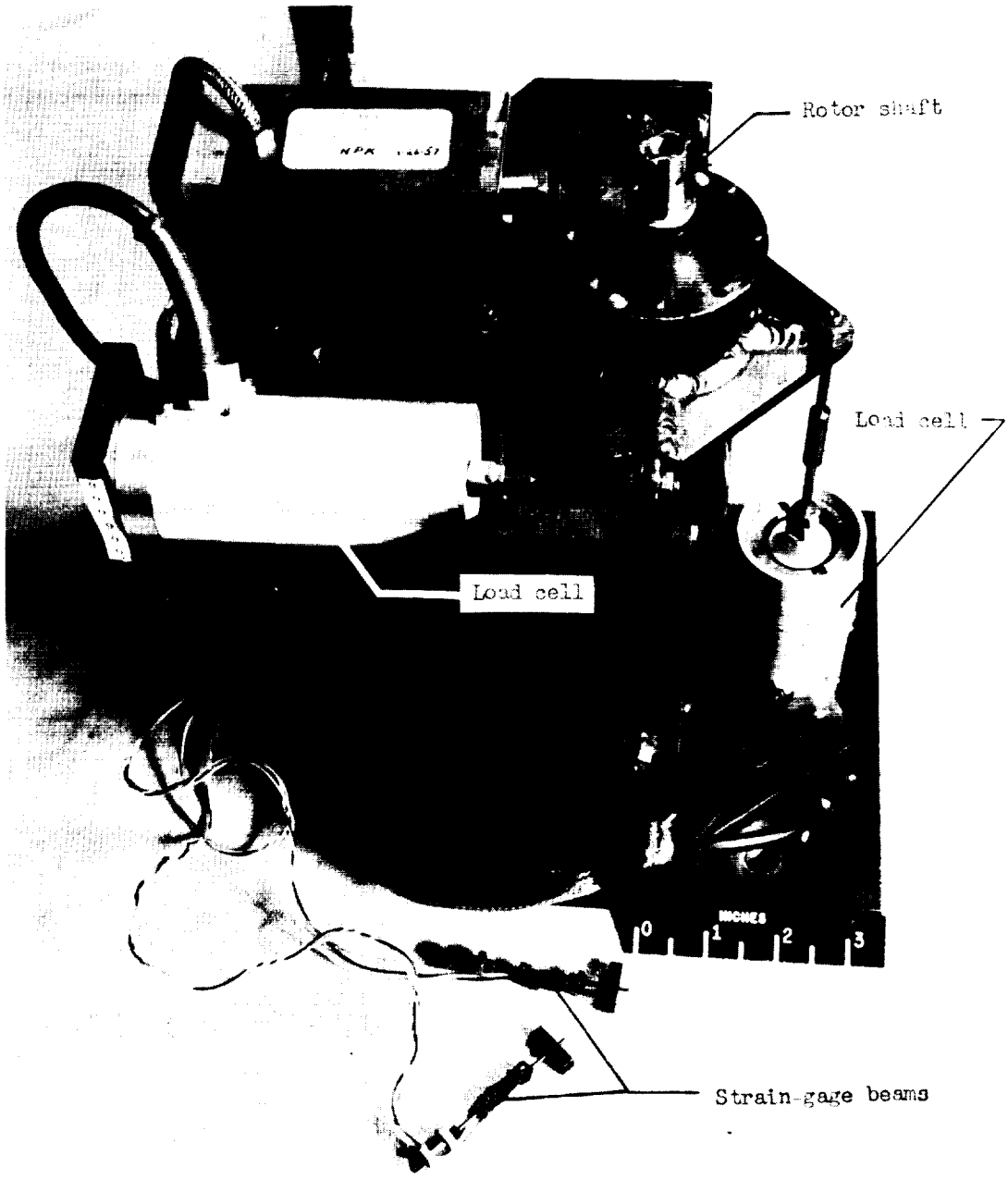

(b) Top view. L-58-1169.1

Figure 7.- Concluded.

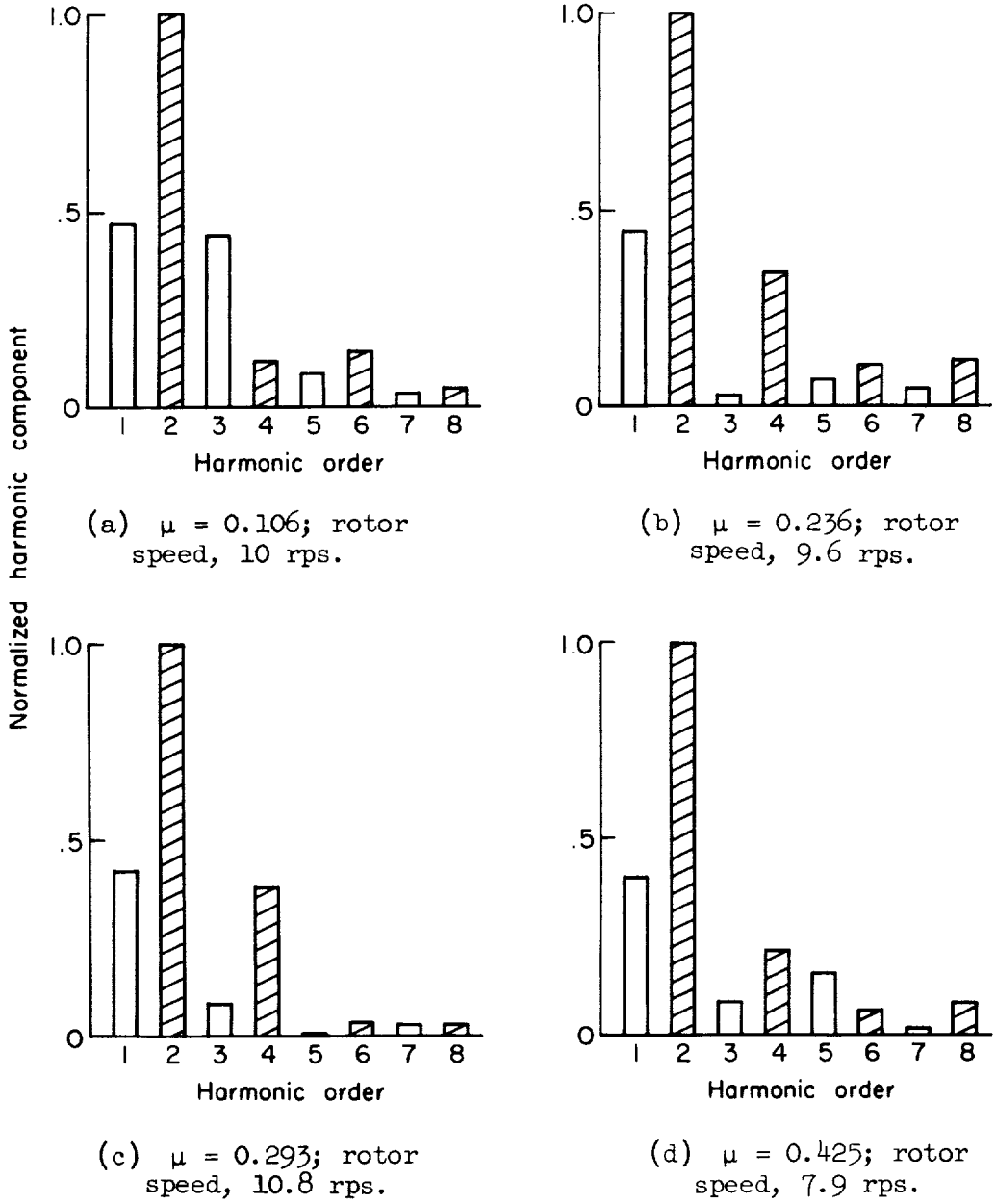

(a) μ = 0.106; rotor speed, 10 rps.

(b) μ = 0.236; rotor speed, 9.6 rps.

(c) μ = 0.293; rotor speed, 10.8 rps.

(d) μ = 0.425; rotor speed, 7.9 rps.

Figure 8.- Harmonic components of thrust loading normalized on principal harmonic for two-blade flapping rotor. (Hatched bars indicate principal harmonic and multiples of the principal harmonic.) $\theta = 0^{\circ}$; $\alpha = -5^{\circ}$.

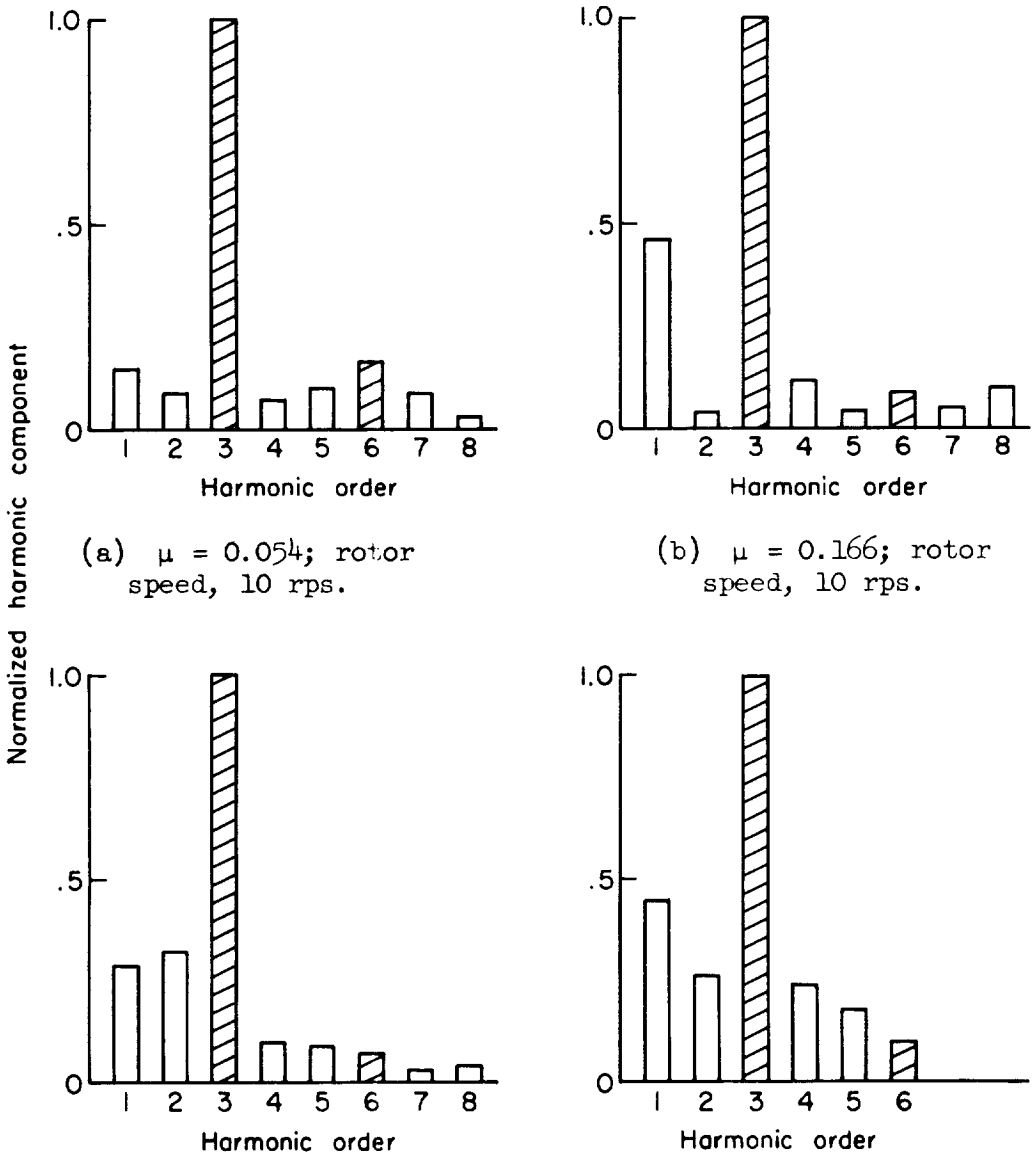

(a) μ = 0.054; rotor speed, 10 rps.

(b) μ = 0.166; rotor speed, 10 rps.

(c) μ = 0.270; rotor speed, 10 rps.

(d) μ = 0.325; rotor speed, 10 rps.

Figure 9.- Harmonic components of thrust loading normalized on principal harmonic for three-blade flapping rotor. (Hatched bars indicate principal harmonic and multiples of the principal harmonic.) $\theta = 3^{\circ}$; $\alpha = 0^{\circ}$.

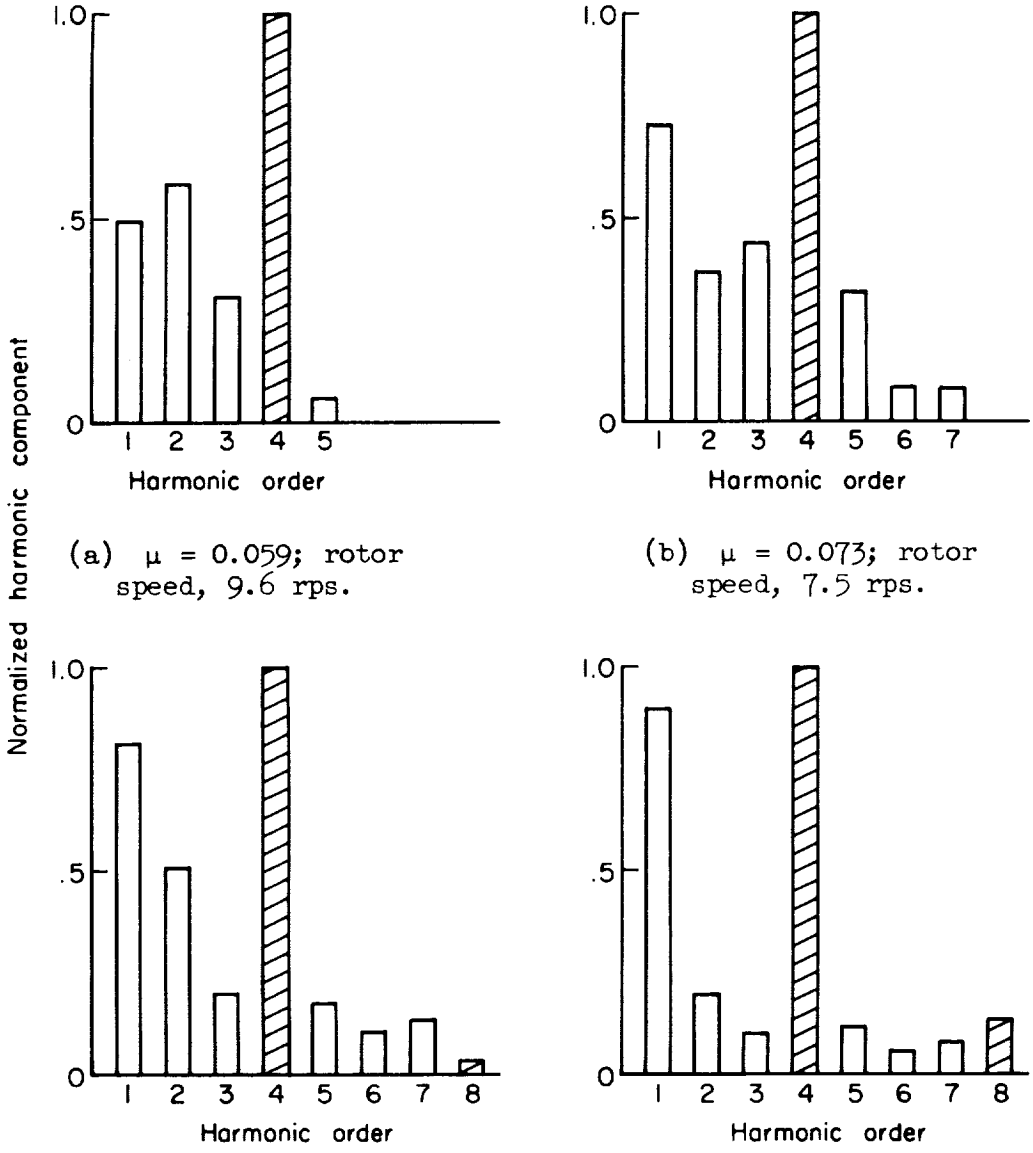

(a) μ = 0.059; rotor speed, 9.6 rps.

(b) μ = 0.073; rotor speed, 7.5 rps.

(c) μ = 0.115; rotor speed, 9.6 rps.

(d) μ = 0.283; rotor speed, 9.6 rps.

Figure 10.- Harmonic components of thrust loading normalized on principal harmonic for four-blade flapping rotor. (Hatched bars indicate principal harmonic and multiples of the principal harmonic.) $\theta = 6^{\circ}$; $\alpha = -10^{\circ}$.

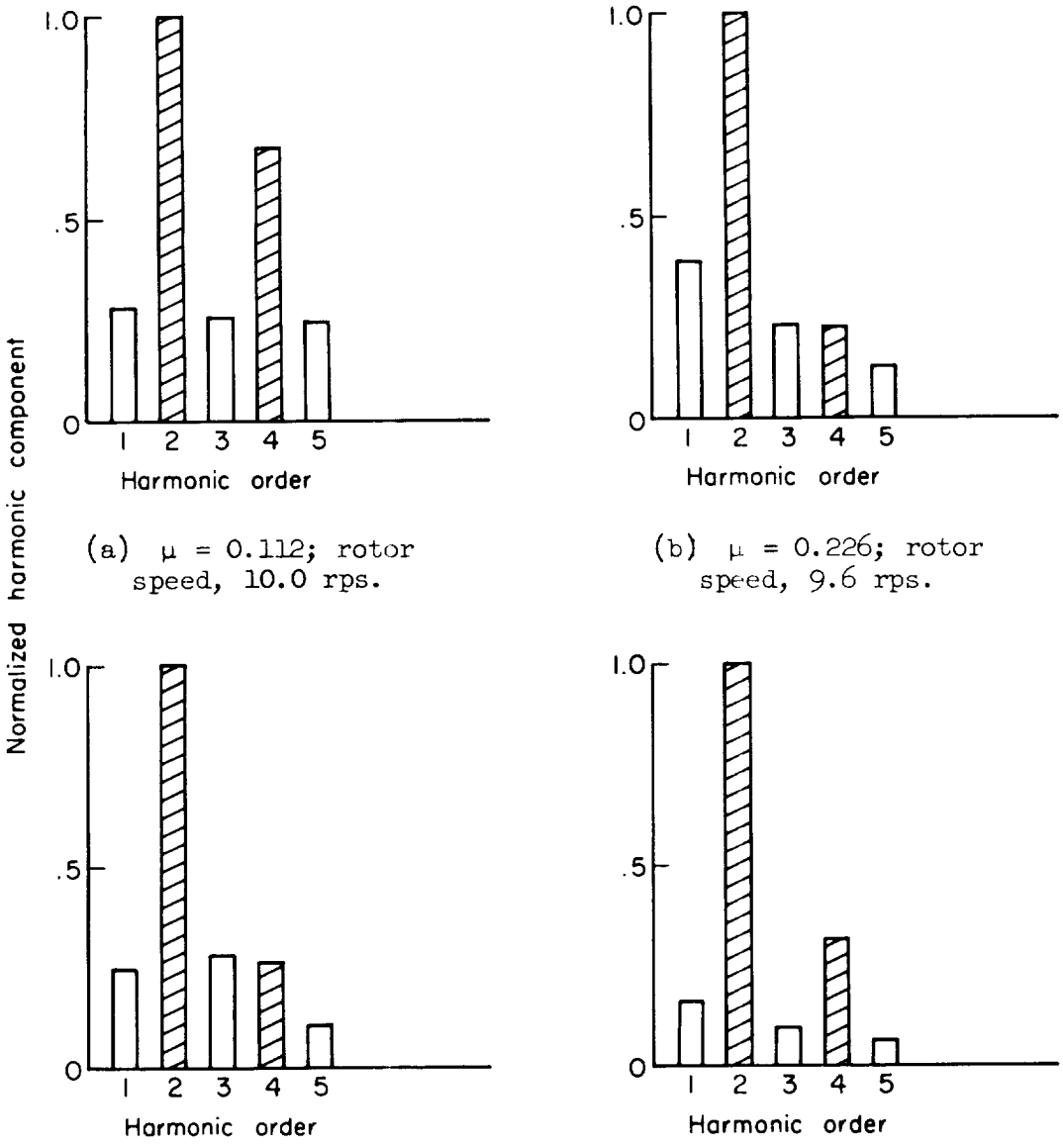

(a) μ = 0.112; rotor speed, 10.0 rps.

(b) μ = 0.226; rotor speed, 9.6 rps.

(c) μ = 0.339; rotor speed, 9.6 rps.

(d) μ = 0.429; rotor speed, 7.5 rps.

Figure 11.- Harmonic components of thrust loading normalized on principal harmonic for two-blade teetering rotor. (Hatched bars indicate principal harmonic and multiples of the principal harmonic.) $\theta = 3^{\circ}$; $\alpha = -5^{\circ}$.

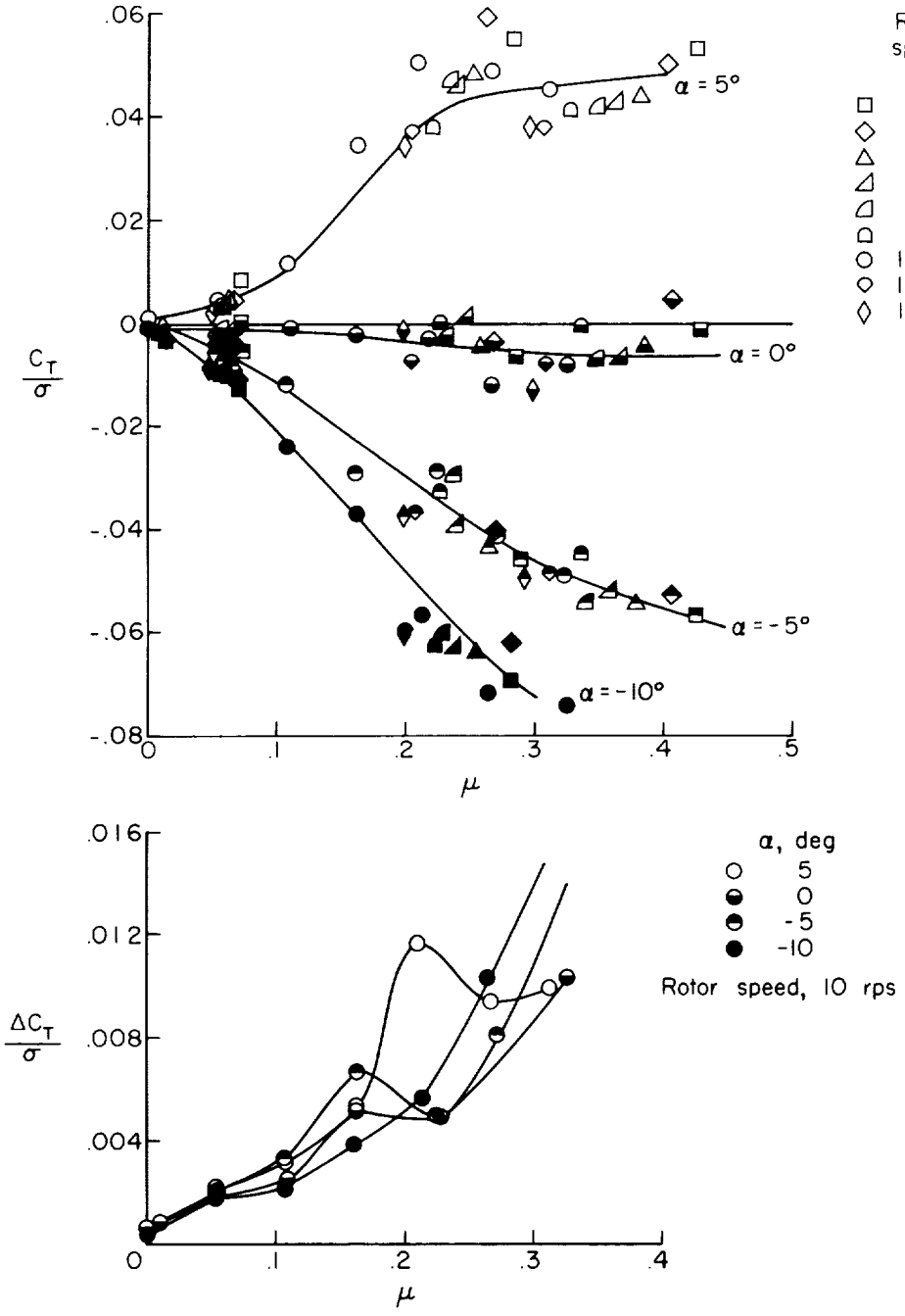

(a) Two-blade flapping rotor.

Figure 12.- Variation of thrust loading coefficient and harmonic periodic components of thrust loading coefficient with tip-speed ratio. $\theta = 0^{\circ}$.

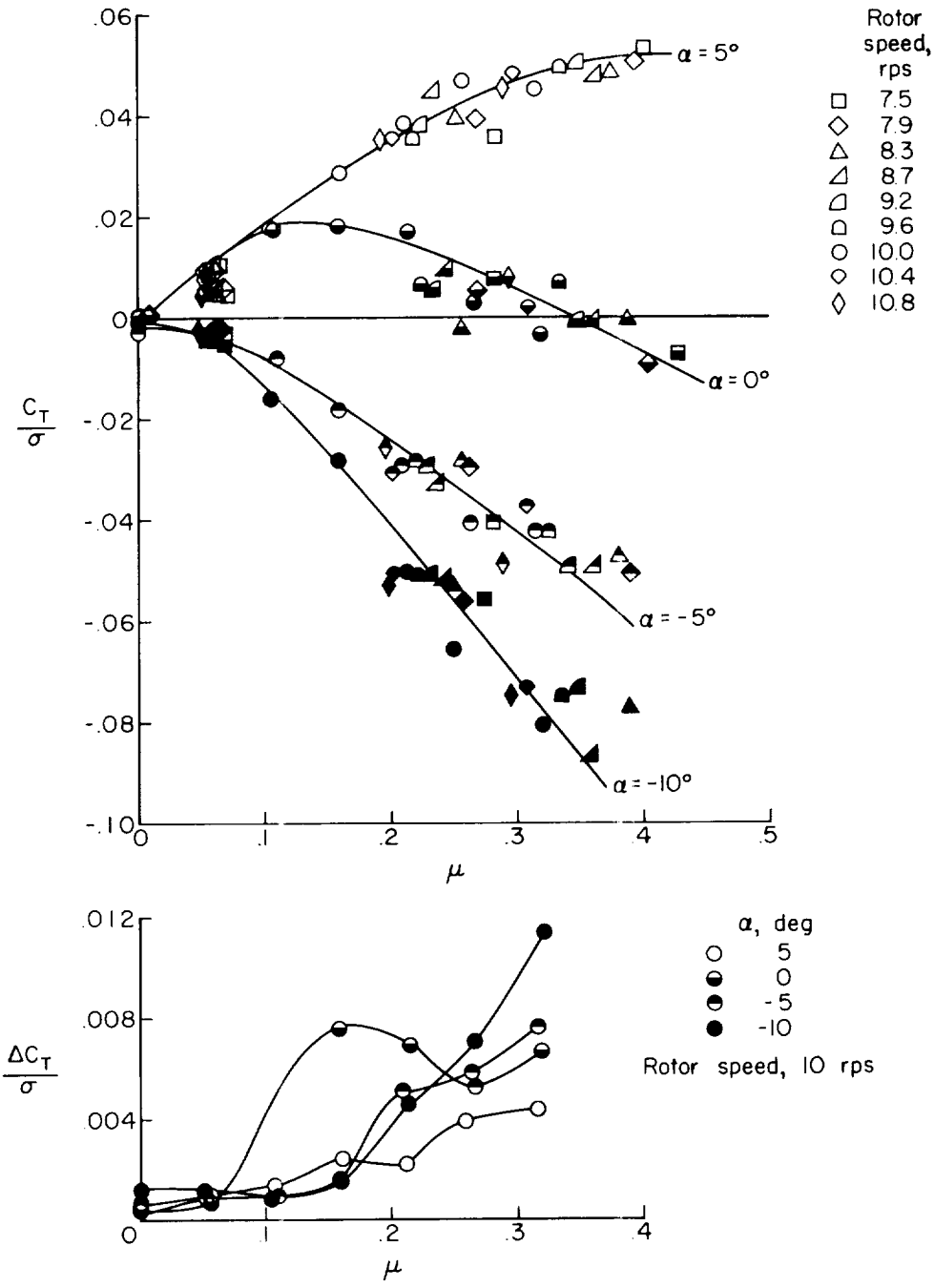

(b) Three-blade flapping rotor.

Figure 12.- Continued.

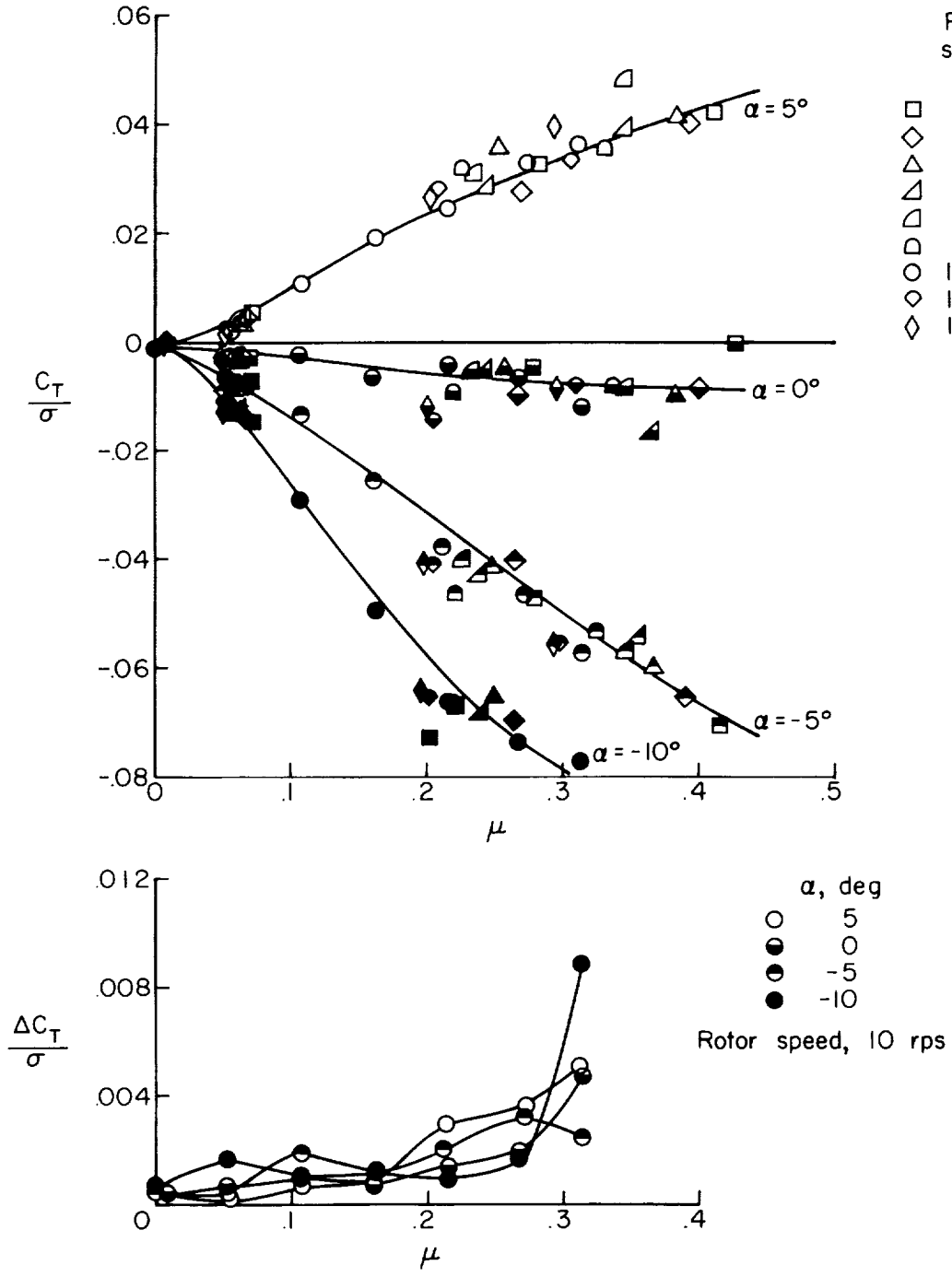

(c) Four-blade flapping rotor.

Figure 12.- Continued.

L-1723

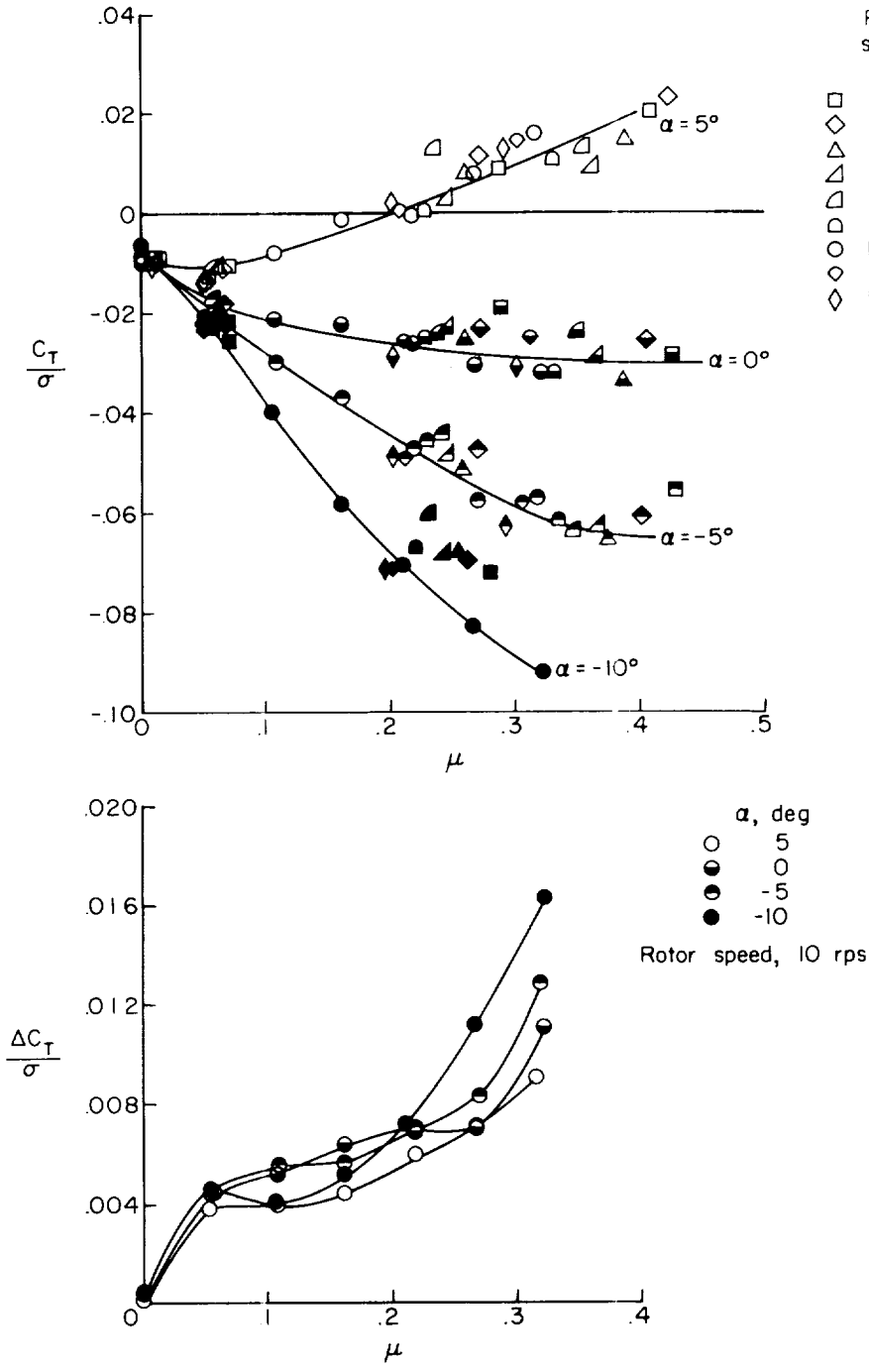

(d) Two-blade teetering rotor.

Figure 12.- Concluded.

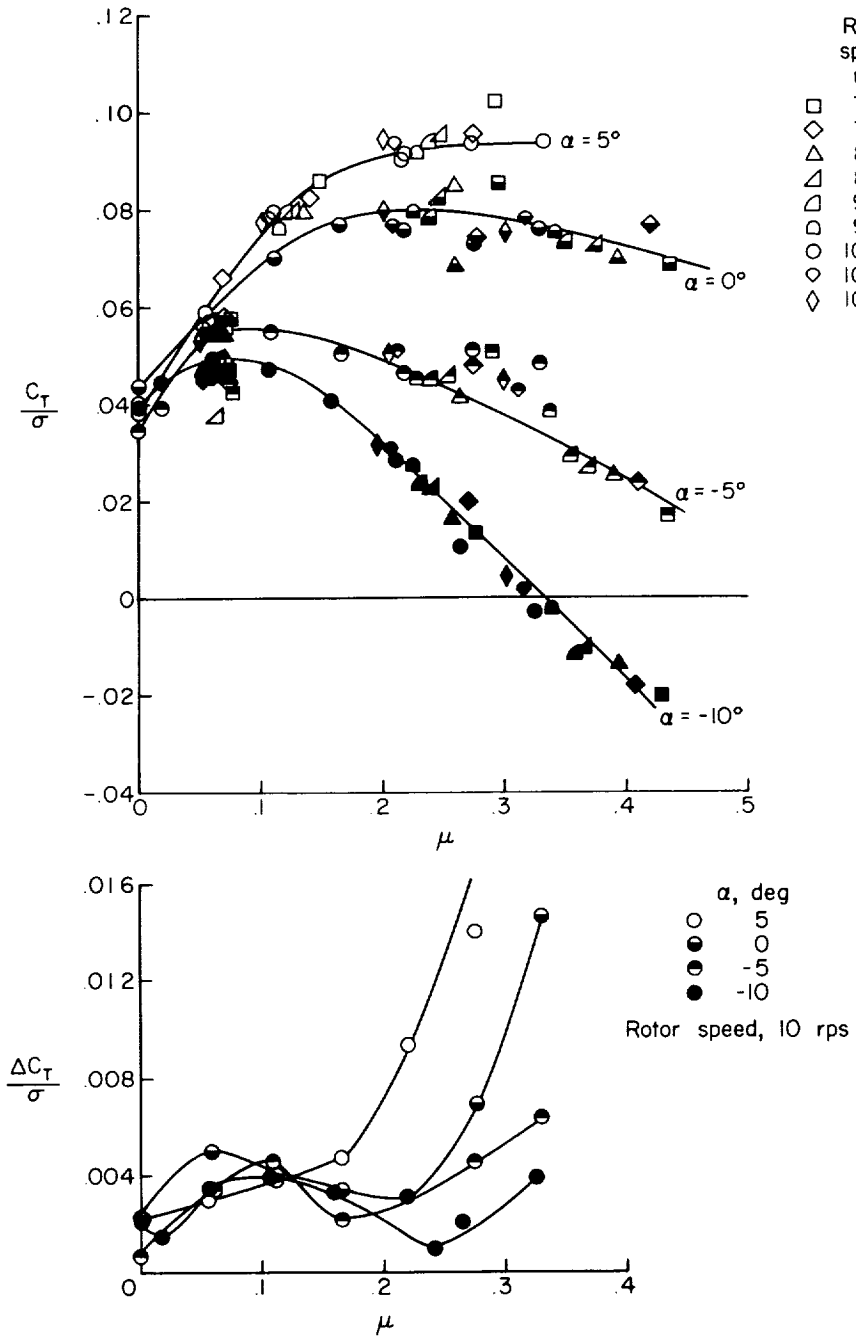

(a) Two-blade flapping rotor.

Figure 13.- Variation of thrust loading coefficient and harmonic periodic components of thrust loading coefficient with tip-speed ratio. $\theta = 3^{\circ}$.

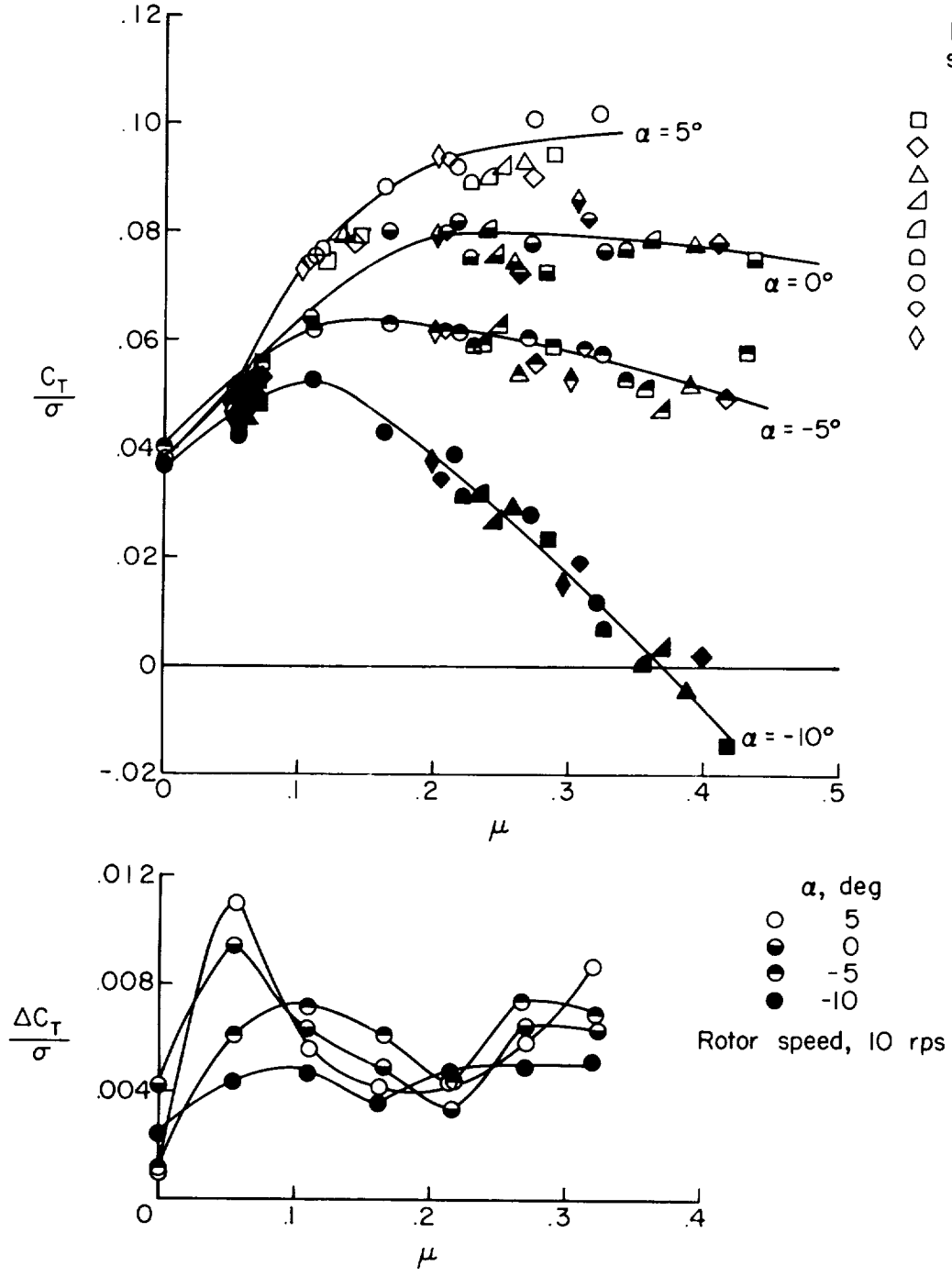

(b) Three-blade flapping rotor.

Figure 13.- Continued.

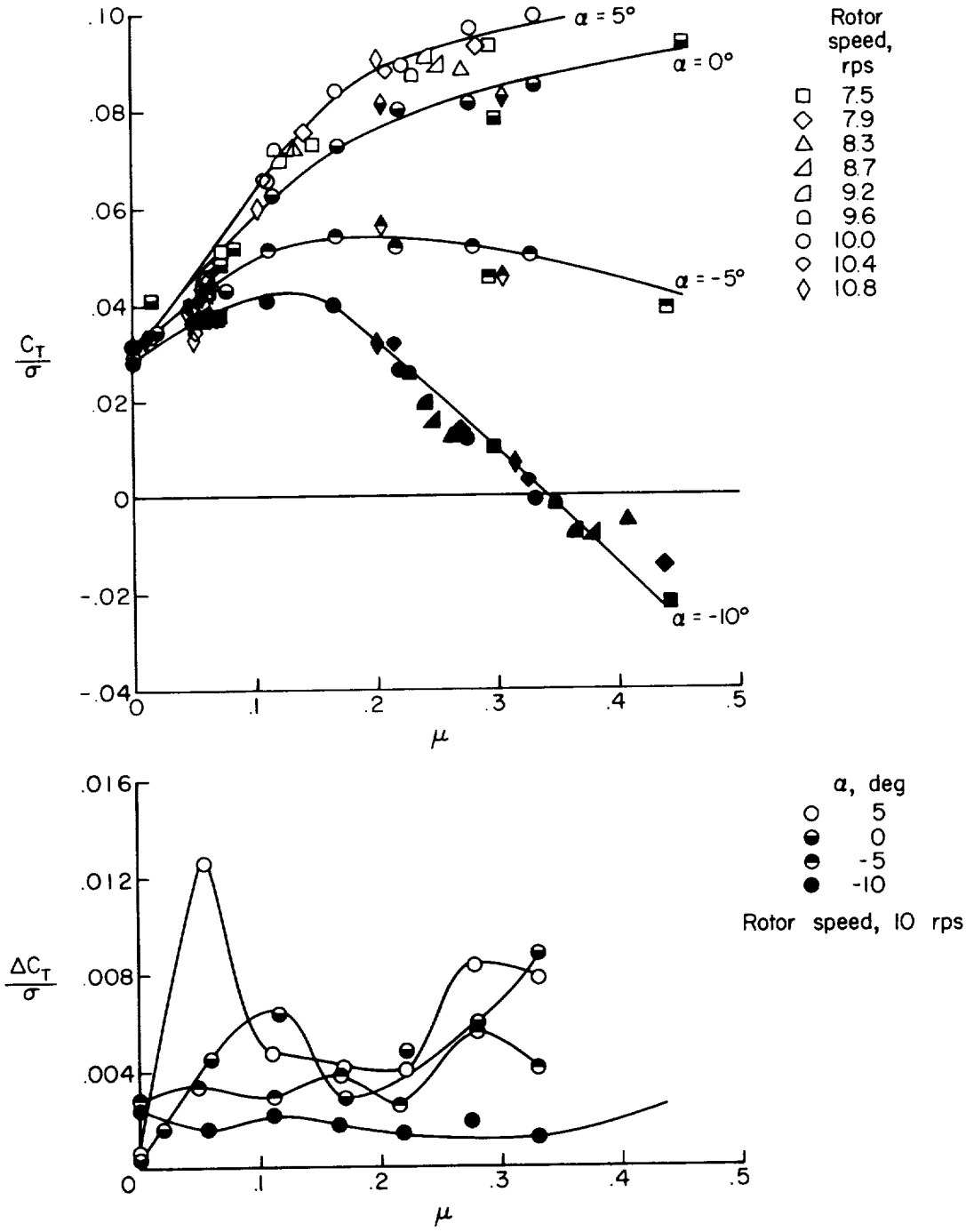

(c) Four-blade flapping rotor.

Figure 13.- Continued.

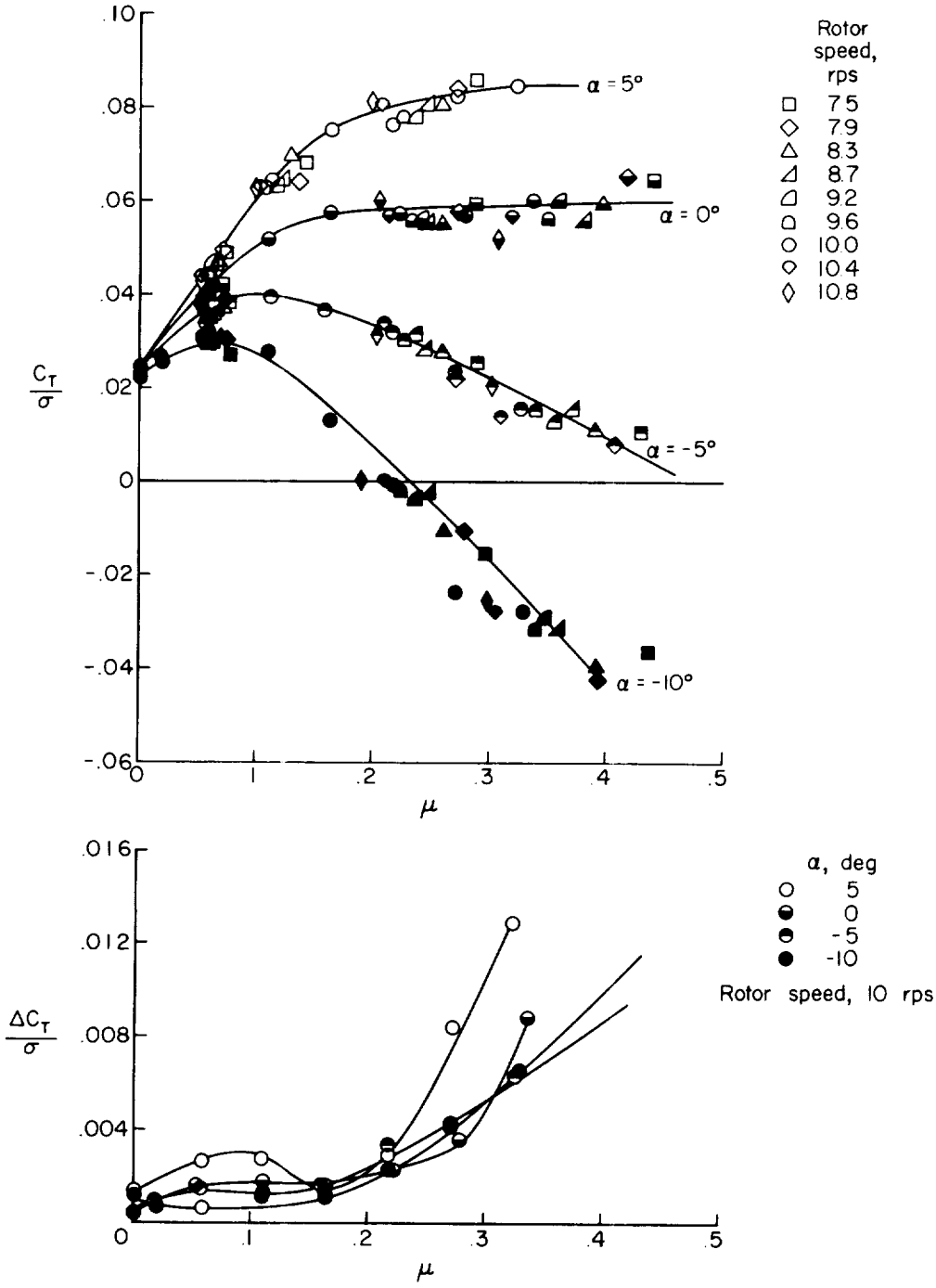

(d) Two-blade teetering rotor.

Figure 13.- Concluded.

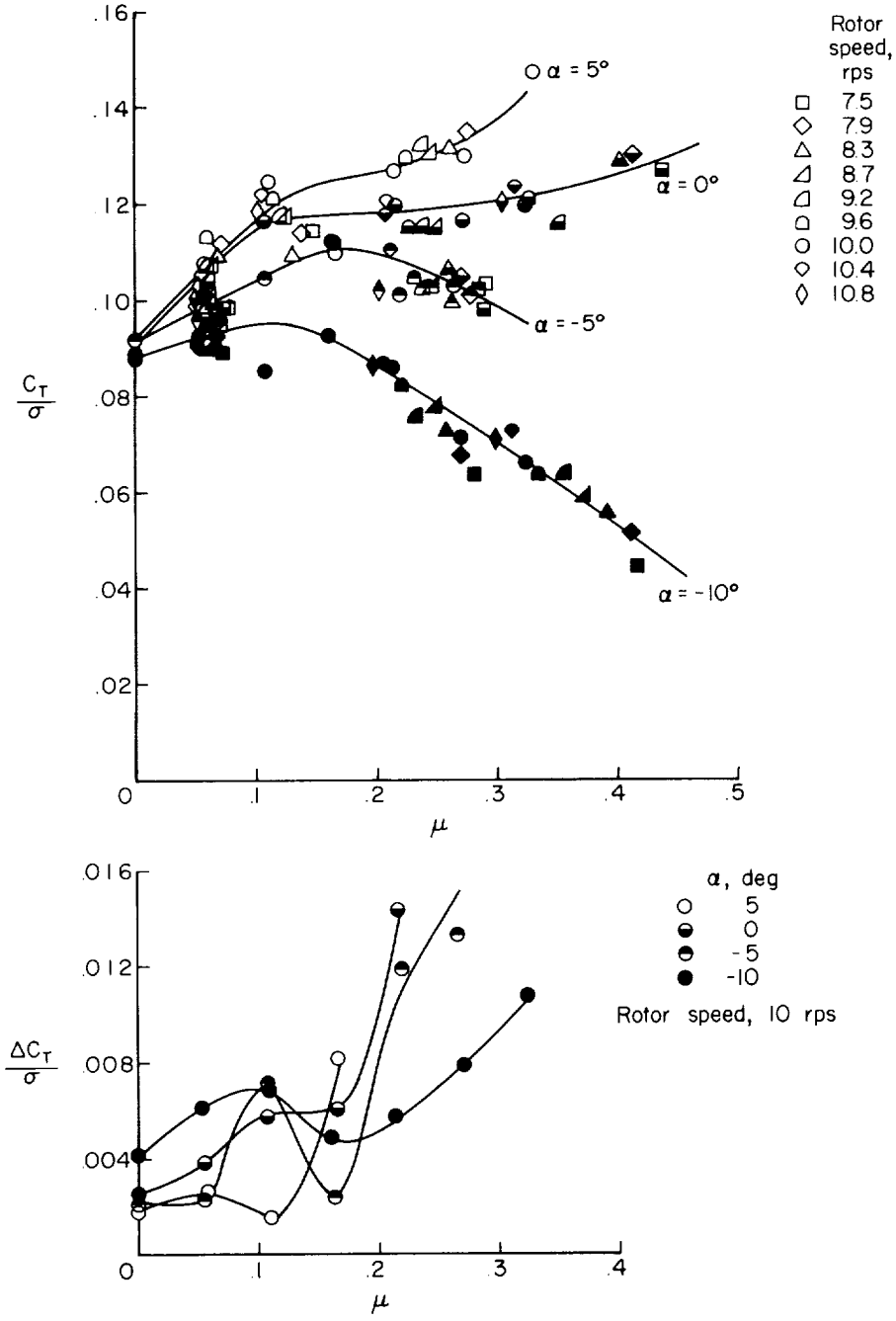

(a) Two-blade flapping rotor.

Figure 14.- Variation of thrust loading coefficient and harmonic periodic components of thrust loading coefficient with tip-speed ratio. $\theta = 6^\circ$.

L-1163

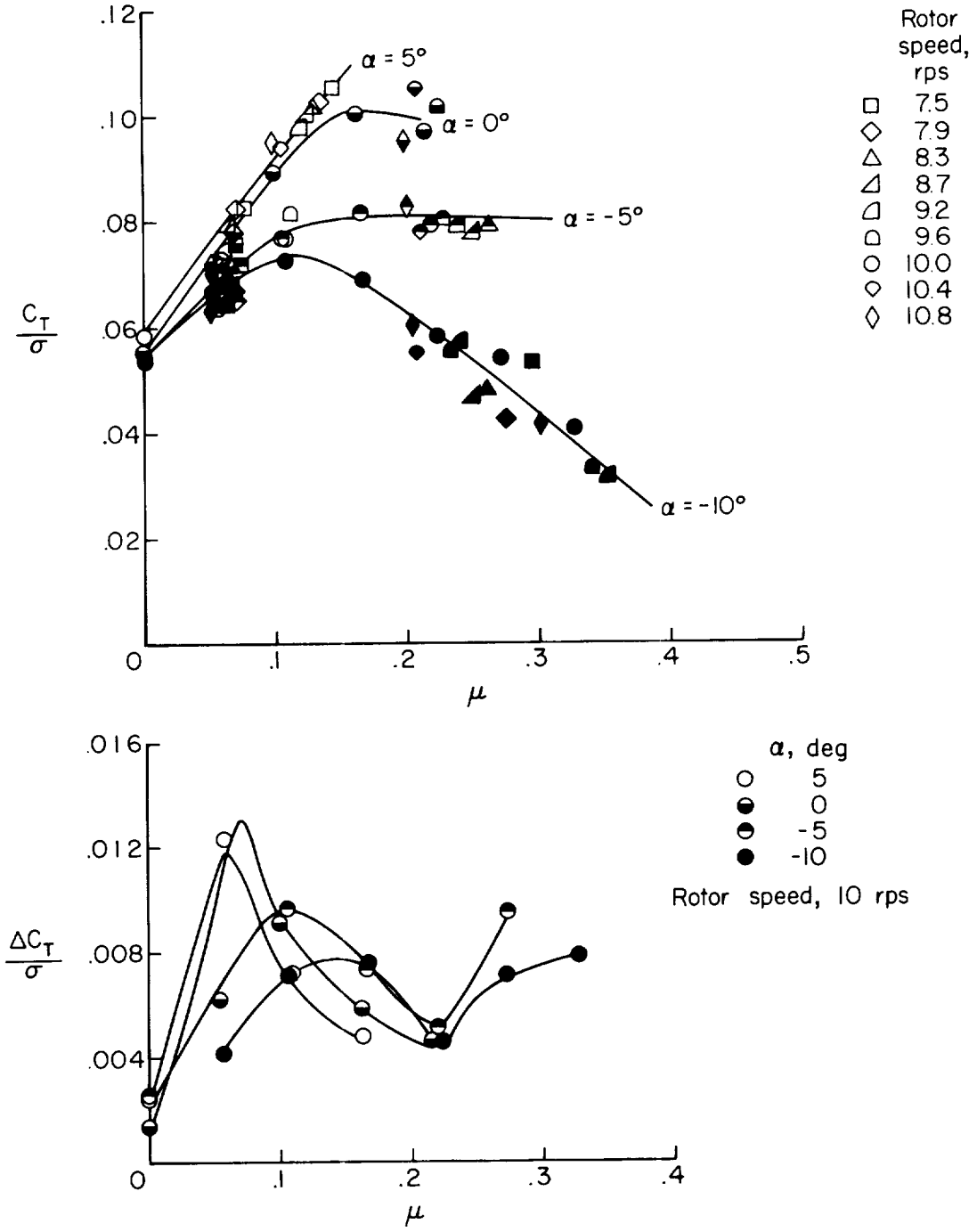

(b) Three-blade flapping rotor.

Figure 14.- Continued.

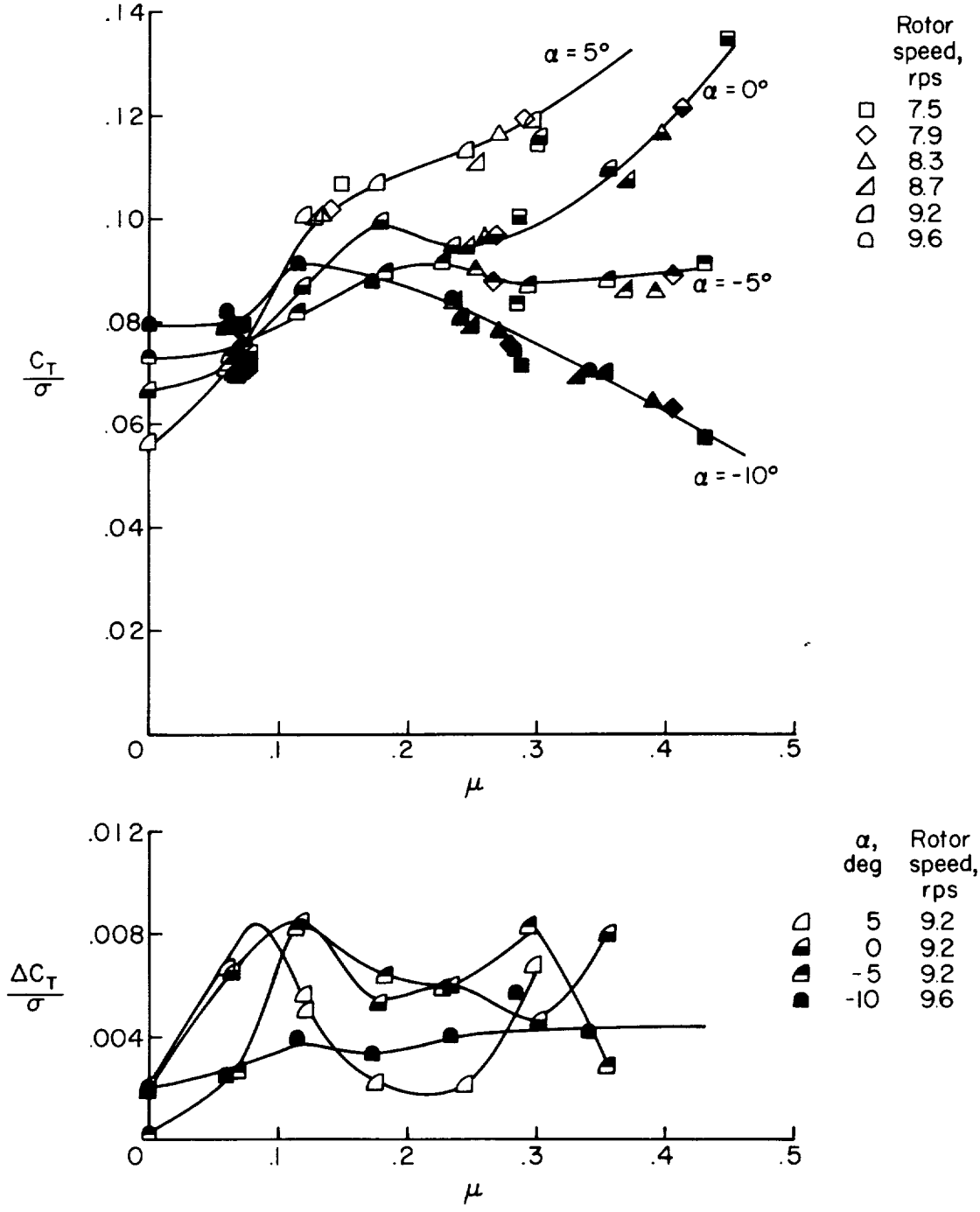

(c) Four-blade flapping rotor.

Figure 14.- Continued.

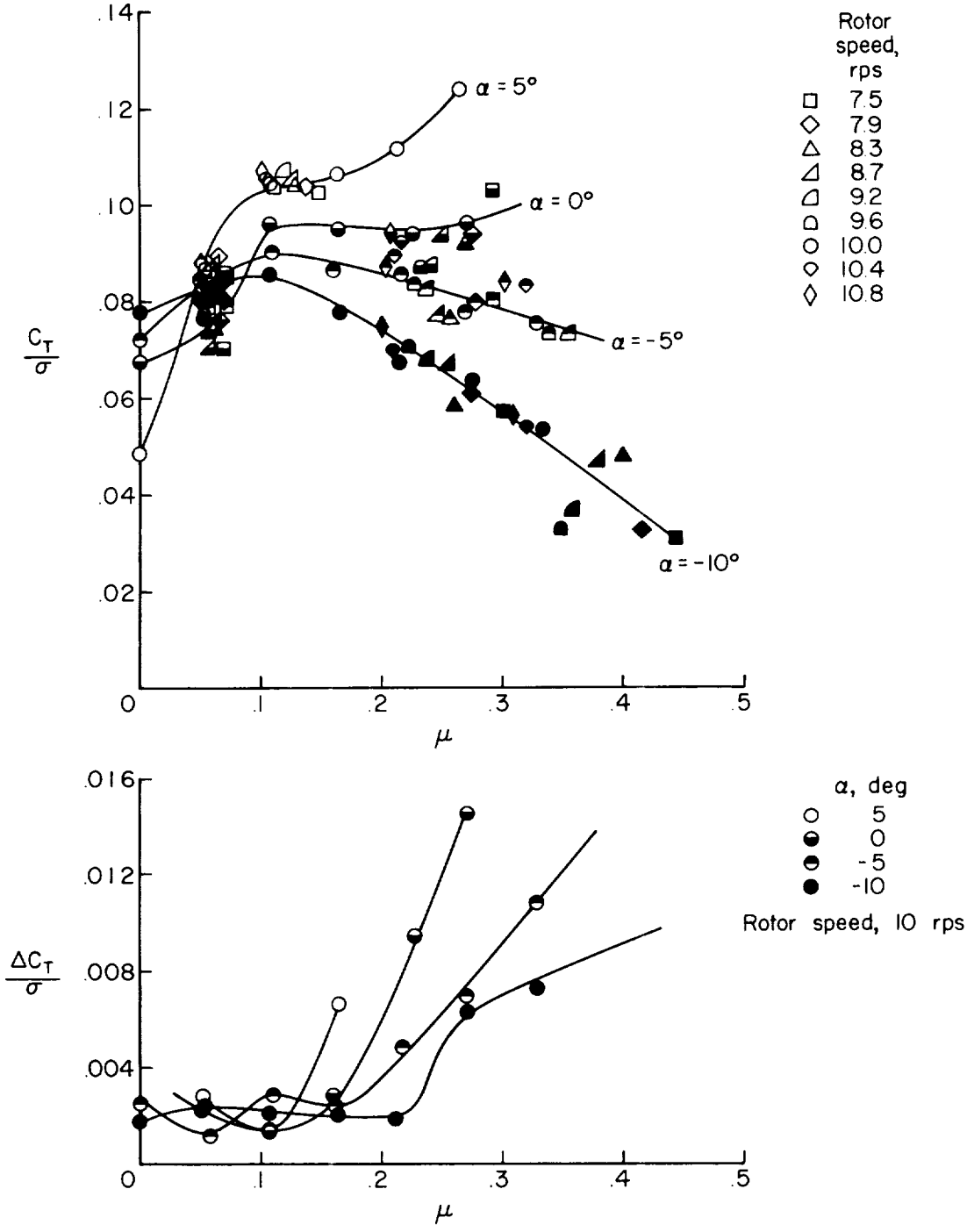

(d) Two-blade teetering rotor.

Figure 14.- Concluded.

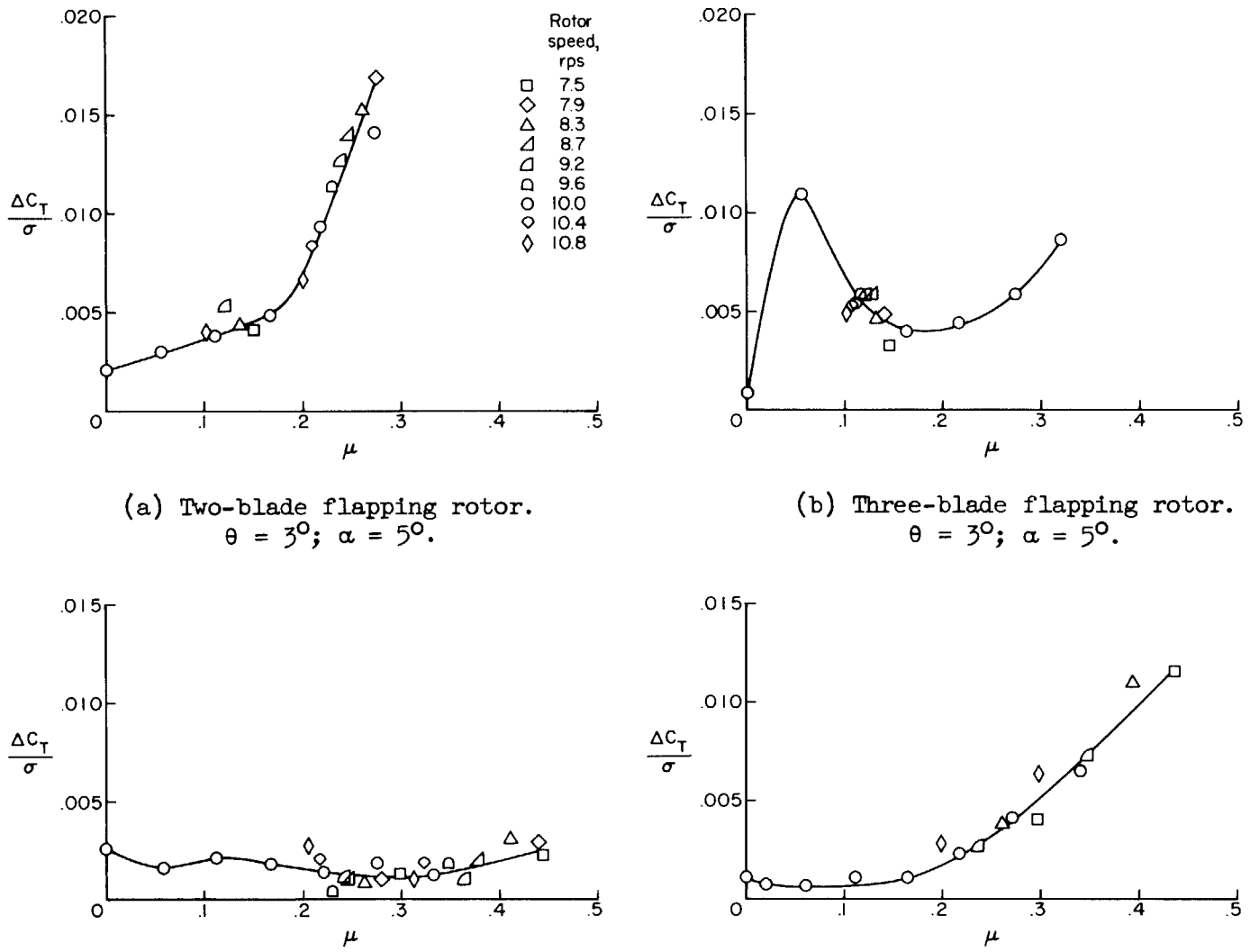

(a) Two-blade flapping rotor. $\theta = 3^\circ$; $\alpha = 5^\circ$.

(b) Three-blade flapping rotor. $\theta = 3^\circ$; $\alpha = 5^\circ$.

(c) Four-blade flapping rotor. $\theta = 3^\circ$; $\alpha = -10^\circ$.

(d) Two-blade teetering rotor. $\theta = 3^\circ$; $\alpha = -10^\circ$.

Figure 15.- Variation of harmonic periodic components of thrust loading coefficient with tip-speed ratio.

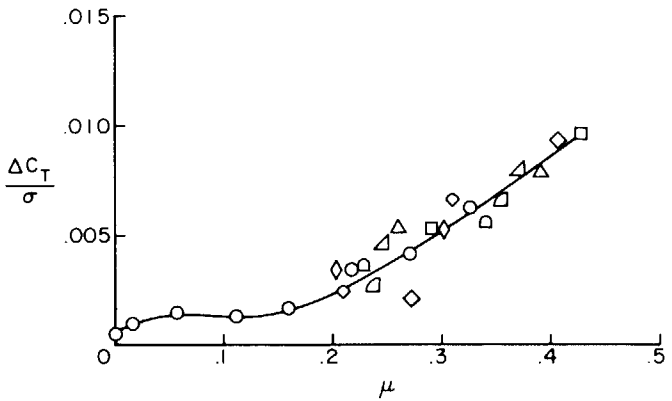

(e) Two-blade teetering rotor.
$\theta = 3^\circ$; $\alpha = -5^\circ$.

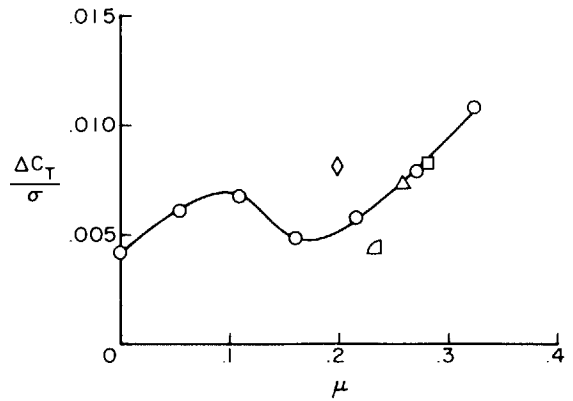

(f) Two-blade flapping rotor.
$\theta = 6^\circ$; $\alpha = -10^\circ$.

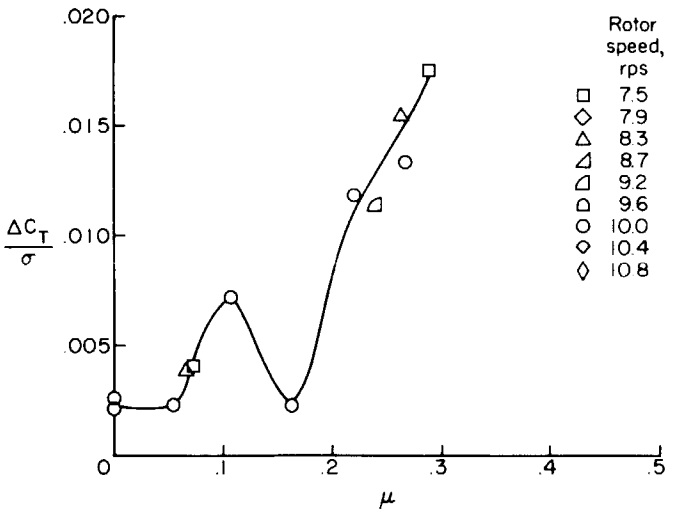

(g) Two-blade flapping rotor.
$\theta = 6^\circ$; $\alpha = -5^\circ$.

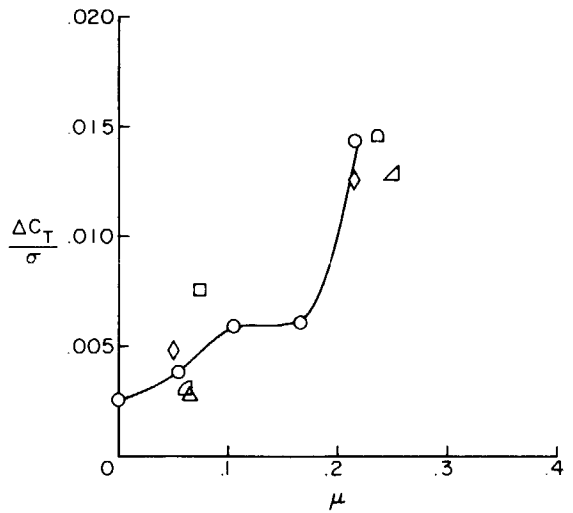

(h) Two-blade flapping rotor.
$\theta = 6^\circ$; $\alpha = 0^\circ$.

Figure 15.- Continued.

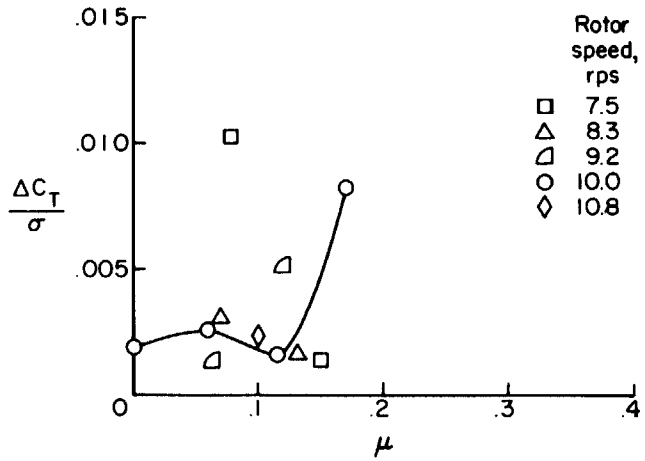

(i) Two-blade flapping rotor. $\theta = 6^{\circ}$; $\alpha = 5^{\circ}$.

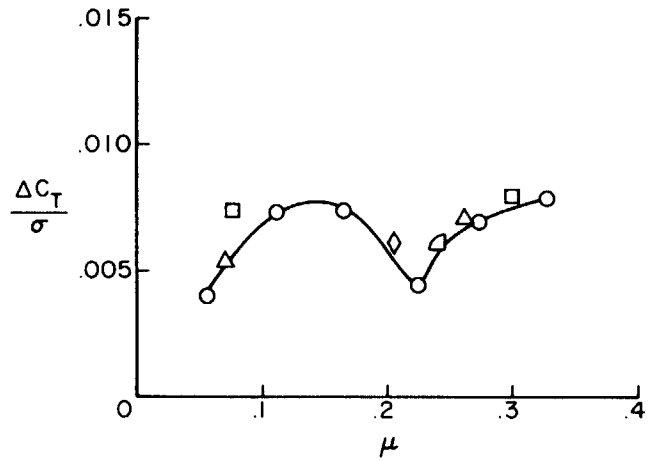

(j) Three-blade flapping rotor. $\theta = 6^{\circ}$, $\alpha = -10^{\circ}$.

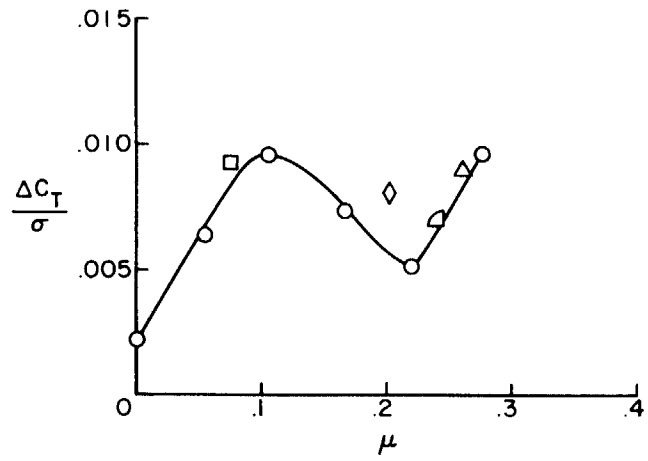

(k) Three-blade flapping rotor. $\theta = 6^{\circ}$; $\alpha = -5^{\circ}$.

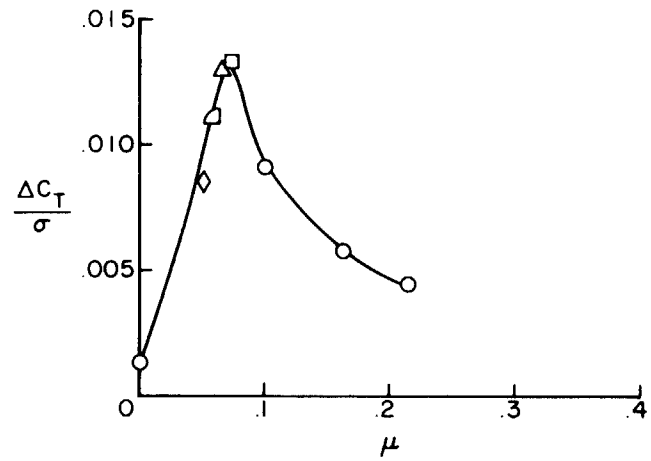

(l) Three-blade flapping rotor. $\theta = 6^{\circ}$; $\alpha = 0^{\circ}$.

Figure 15.- Continued.

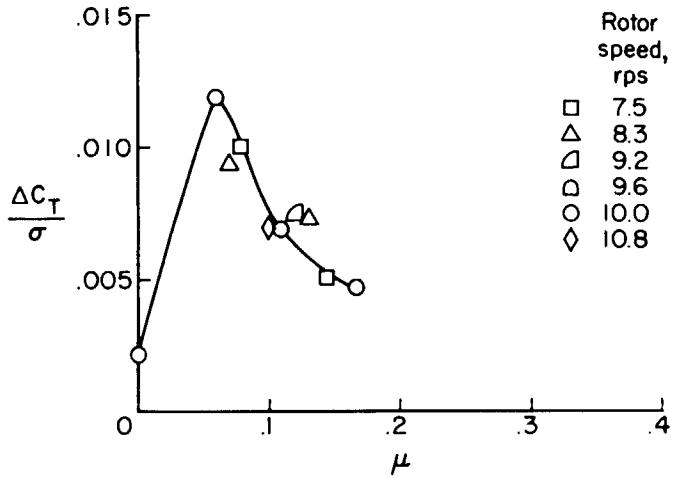

(m) Three-blade flapping rotor.
$\theta = 6^\circ$; $\alpha = 5^\circ$.

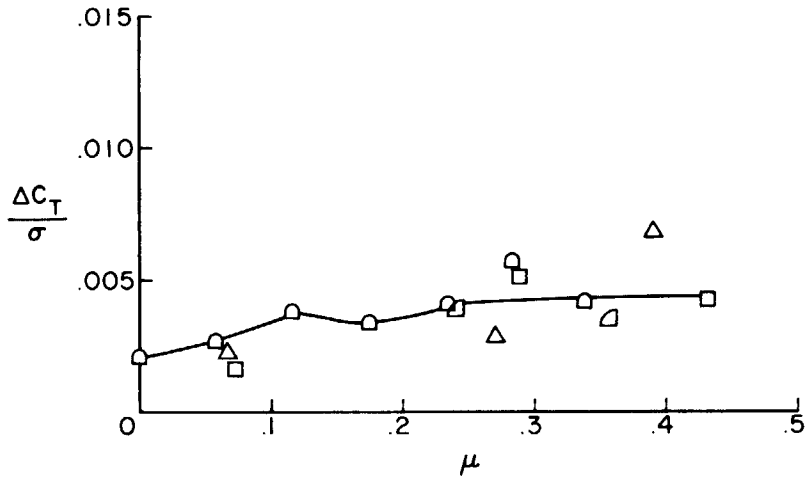

(n) Four-blade flapping rotor.
$\theta = 6^\circ$; $\alpha = -10^\circ$.

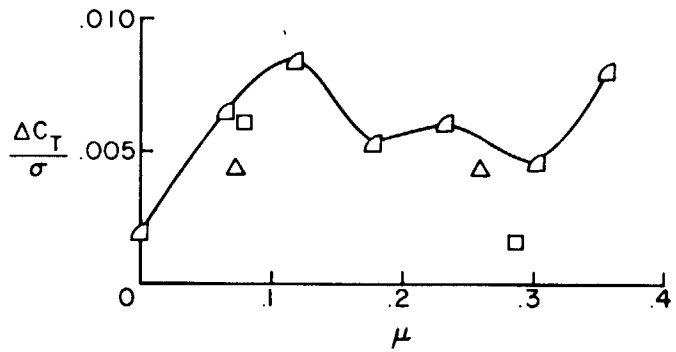

(o) Four-blade flapping rotor.
$\theta = 6^\circ$; $\alpha = 0^\circ$.

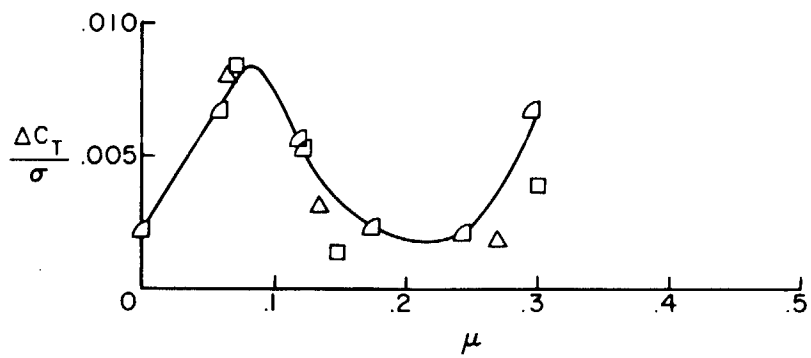

(p) Four-blade flapping rotor.
$\theta = 6^\circ$; $\alpha = 5^\circ$.

Figure 15.- Continued.

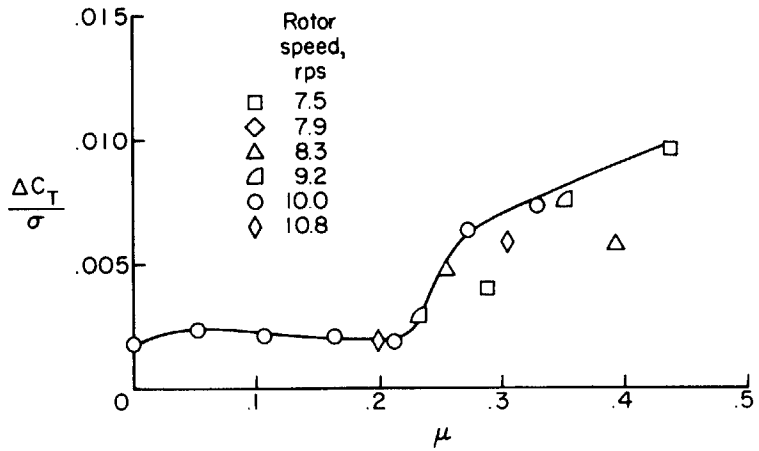

(q) Two-blade teetering rotor.
$\theta = 6^\circ$; $\alpha = -10^\circ$.

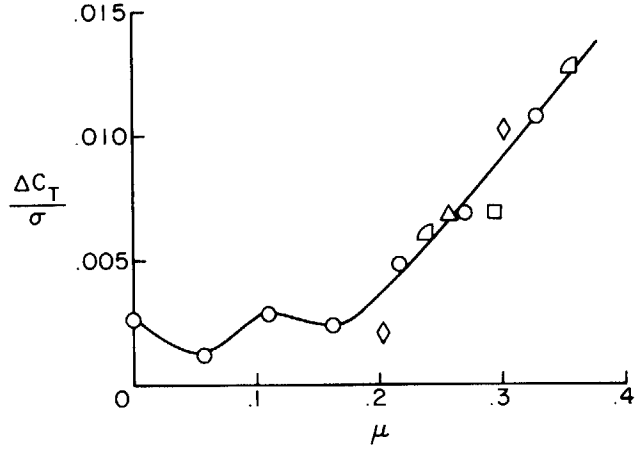

(r) Two-blade teetering rotor.
$\theta = 6^\circ$; $\alpha = -5^\circ$.

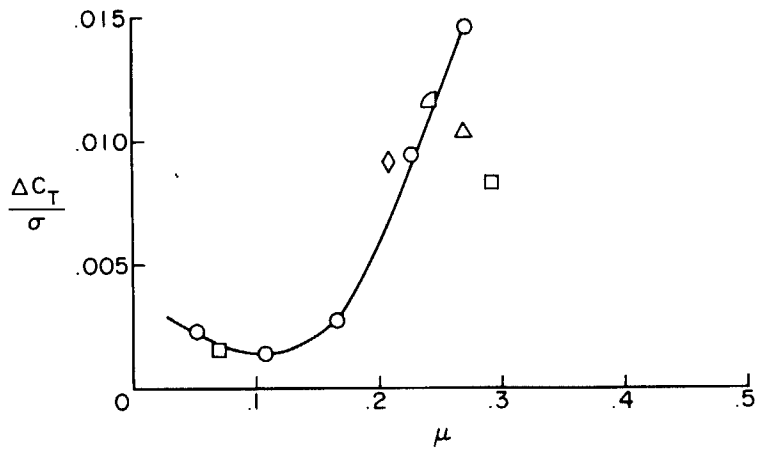

(s) Two-blade teetering rotor
$\theta = 6^\circ$; $\alpha = 0^\circ$.

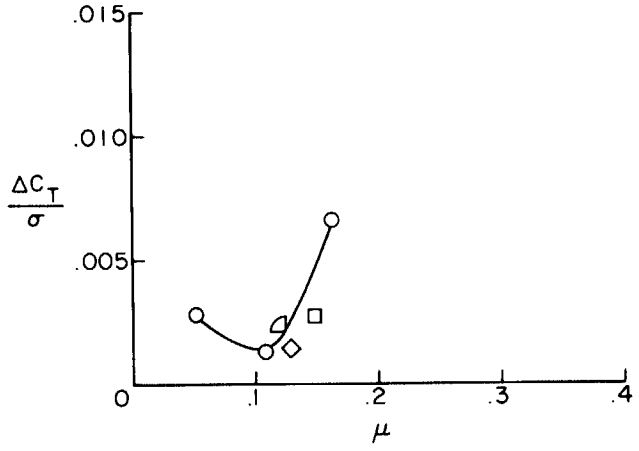

(t) Two-blade teetering rotor.
$\theta = 6^\circ$; $\alpha = 5^\circ$.

Figure 15.- Concluded.

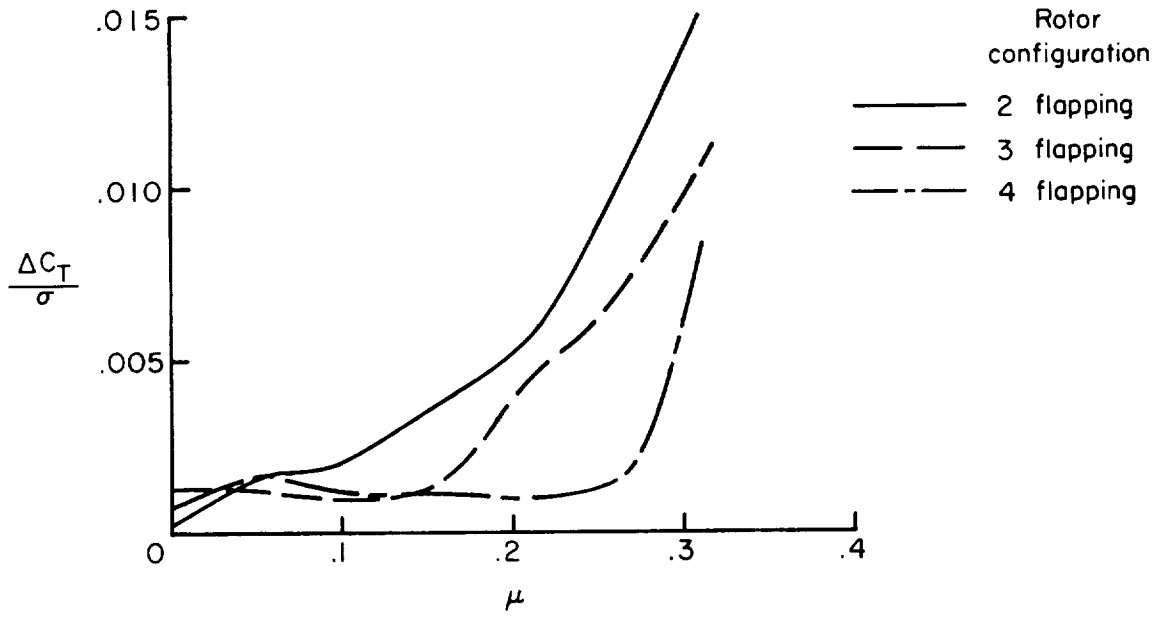

(a) $\theta = 0^\circ$; $\alpha = -10^\circ$.

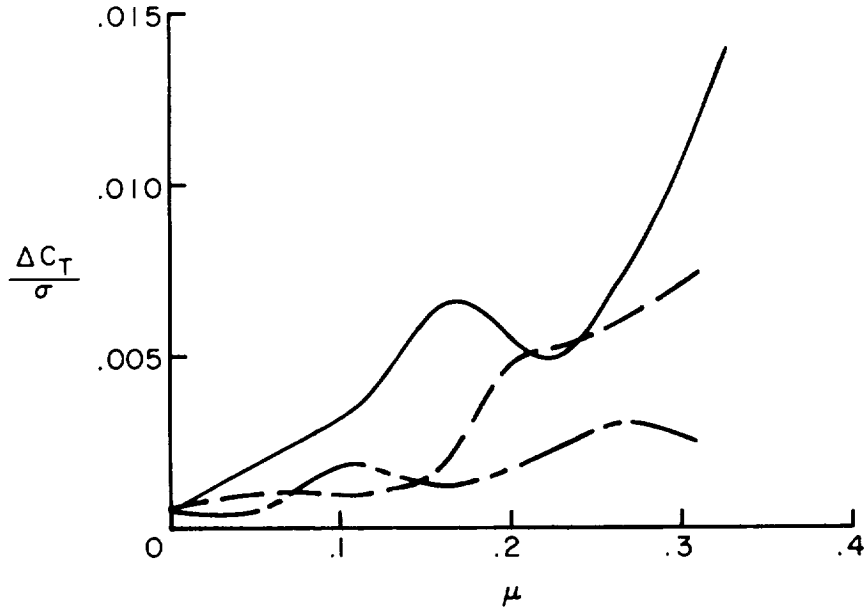

(b) $\theta = 0^\circ$; $\alpha = -5^\circ$.

Figure 16.- Comparison of the principal harmonic periodic components of thrust loading coefficient for various rotor configurations.

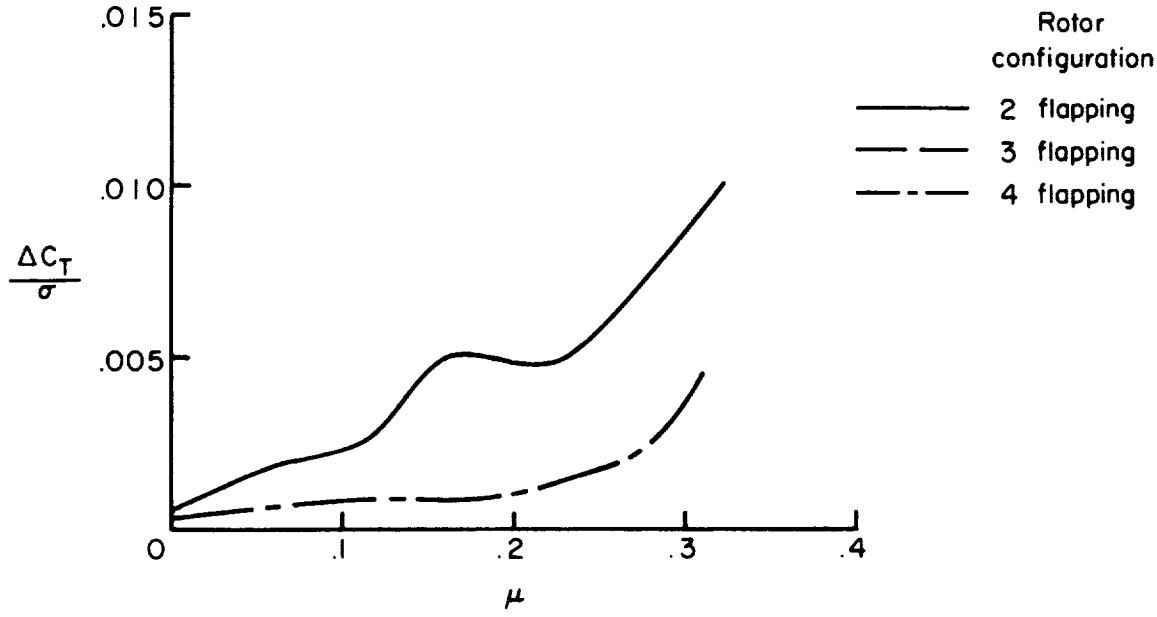

(c) $\theta = 0^\circ$; $\alpha = 0^\circ$.

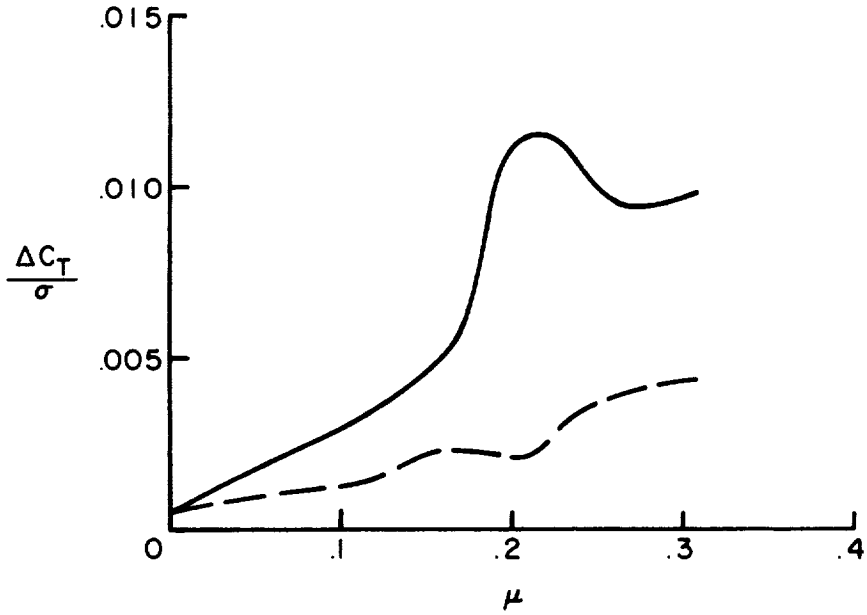

(d) $\theta = 0^\circ$; $\alpha = 5^\circ$.

Figure 16.- Continued.

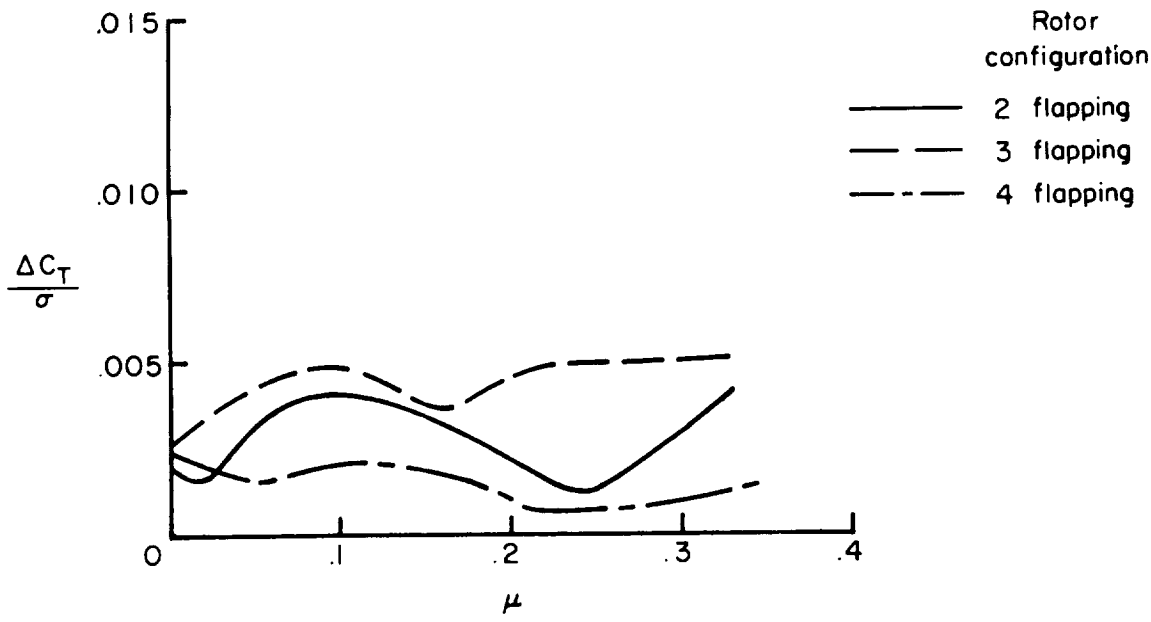

(e) $\theta = 3^\circ$; $\alpha = -10^\circ$.

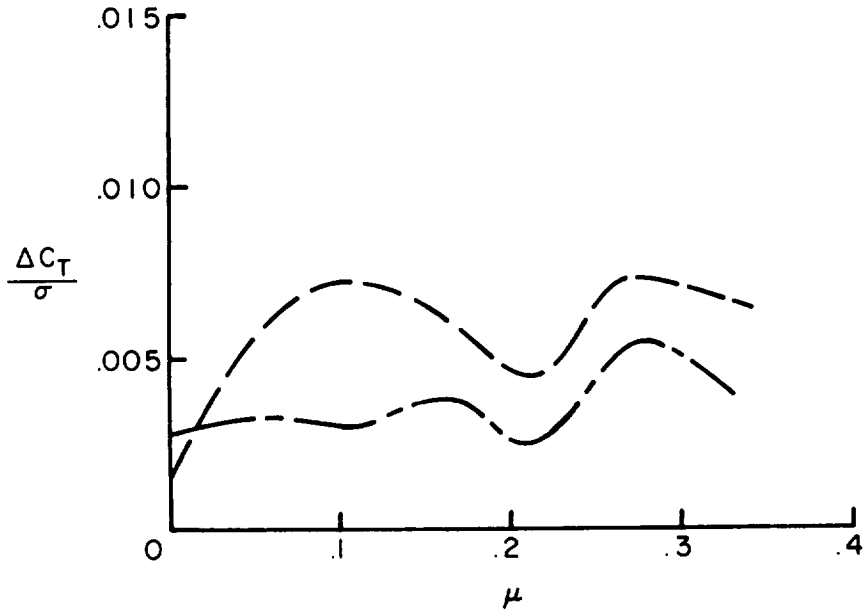

(f) $\theta = 3^\circ$; $\alpha = -5^\circ$.

Figure 16.- Continued.

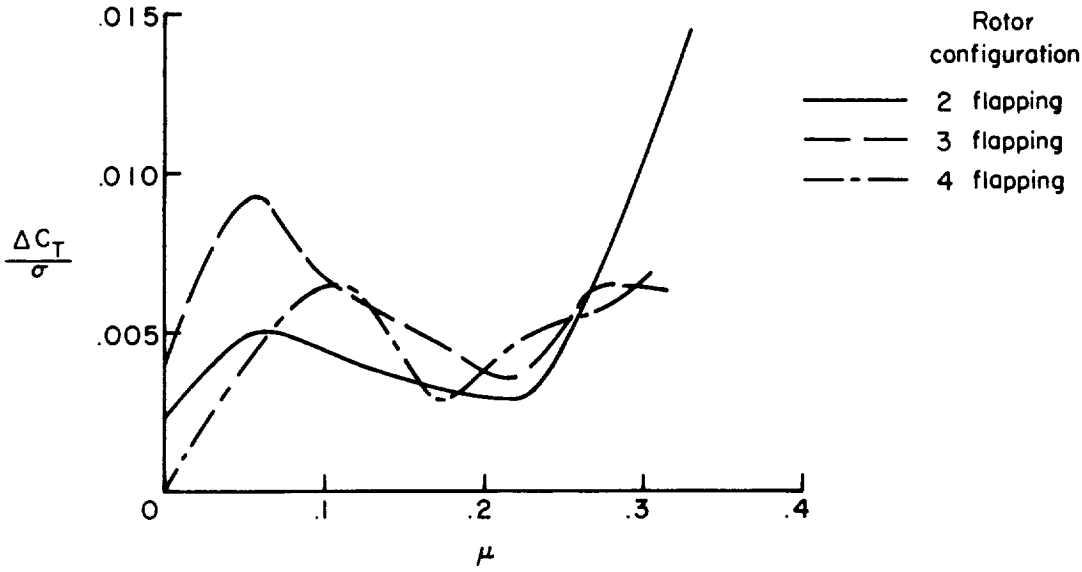

(g) $\theta = 3^\circ$; $\alpha = 0^\circ$.

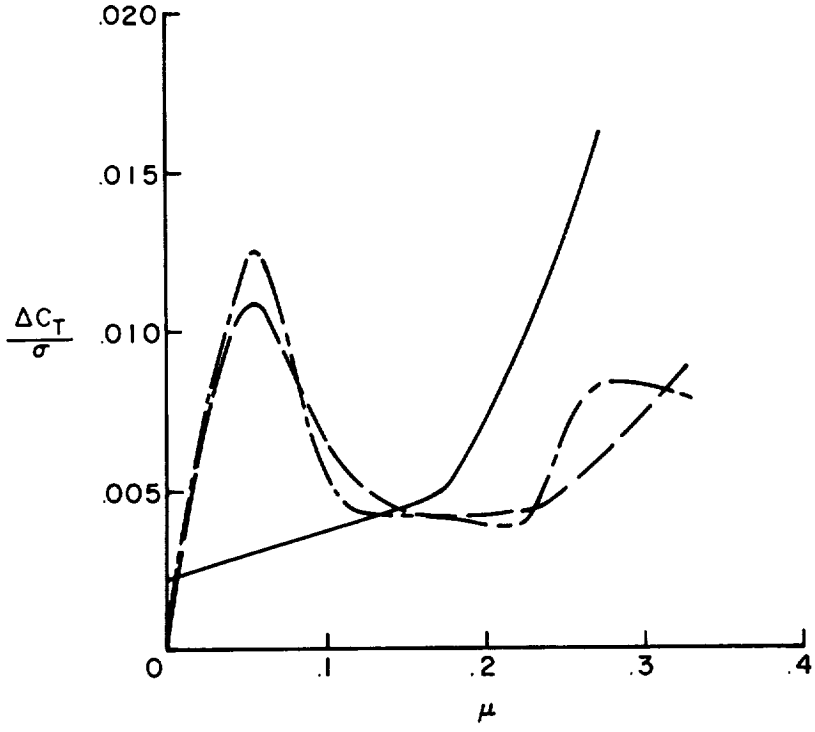

(h) $\theta = 3^\circ$; $\alpha = 5^\circ$.

Figure 16.- Continued.

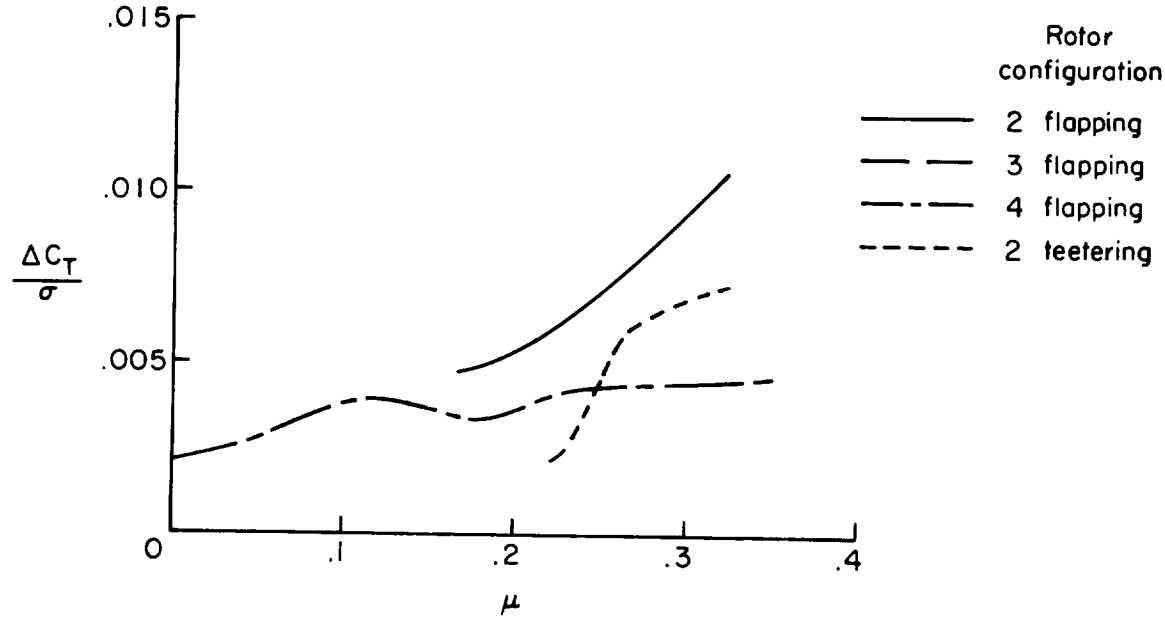

(i) $\theta = 6^\circ$; $\alpha = -10^\circ$.

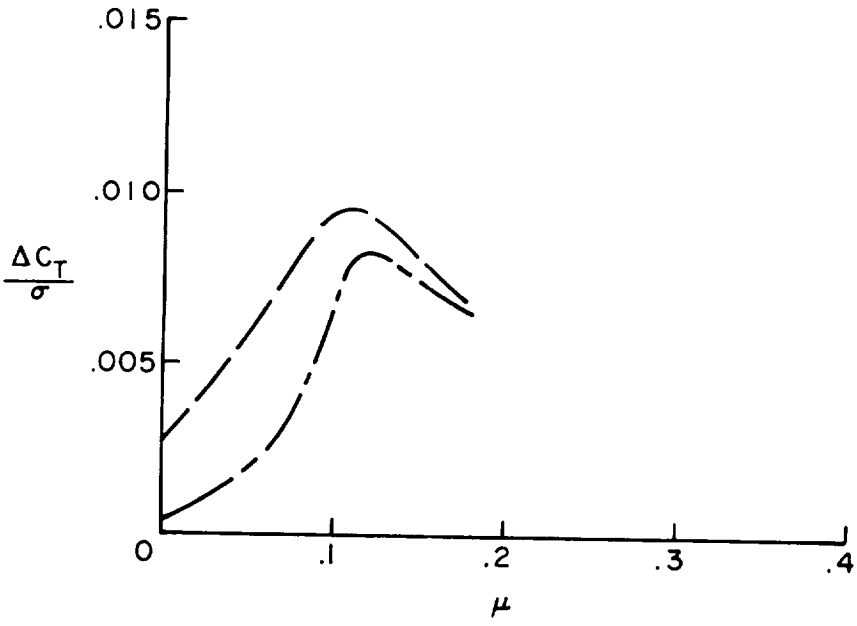

(j) $\theta = 6^\circ$; $\alpha = -5^\circ$.

Figure 16.- Continued.

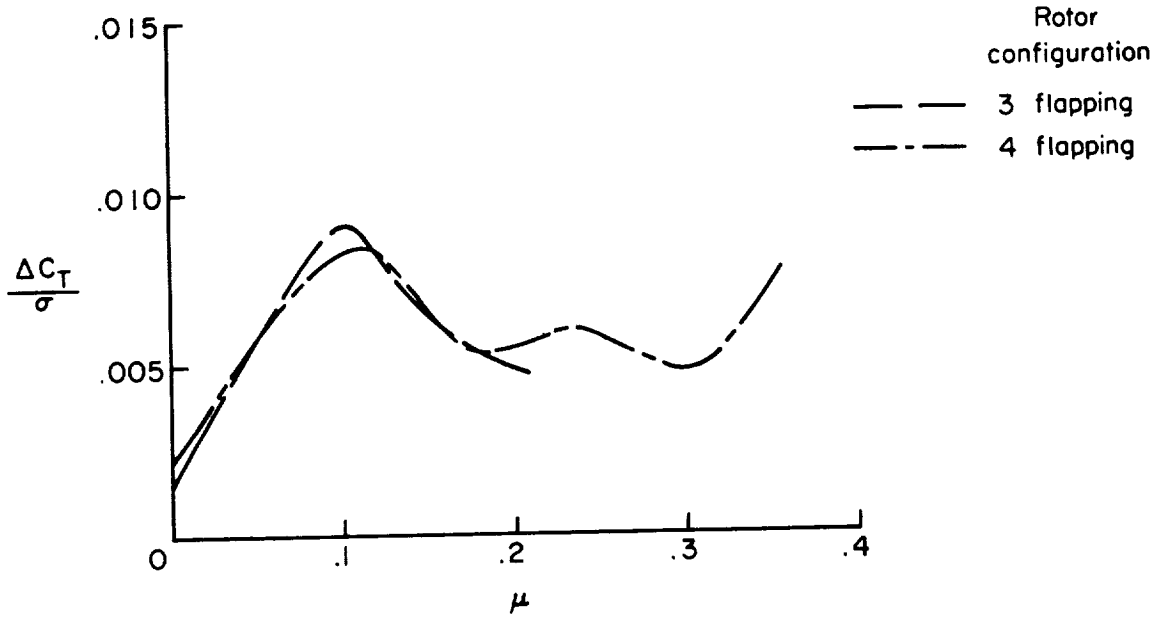

(k) $\theta = 6^\circ$; $\alpha = 0^\circ$.

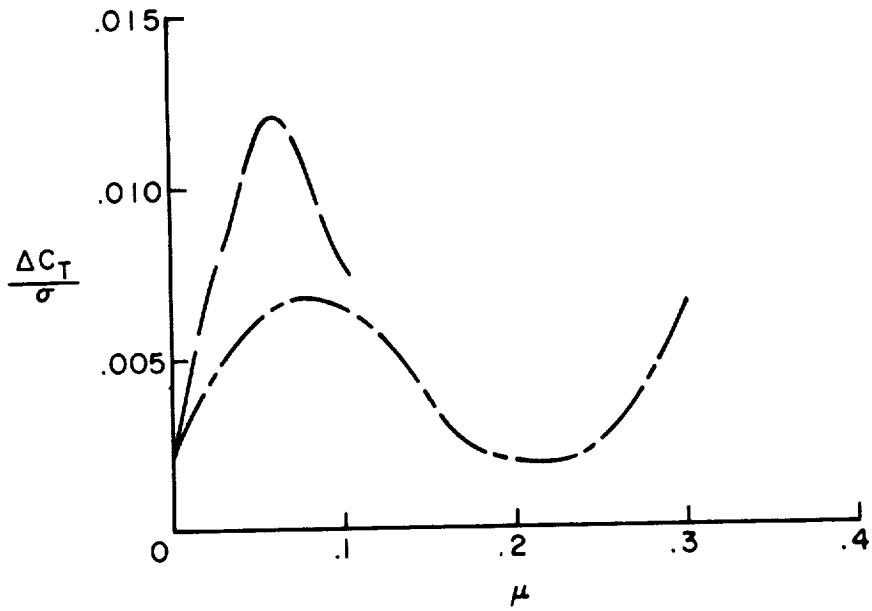

(l) $\theta = 6^\circ$; $\alpha = 5^\circ$.

Figure 16.- Concluded.

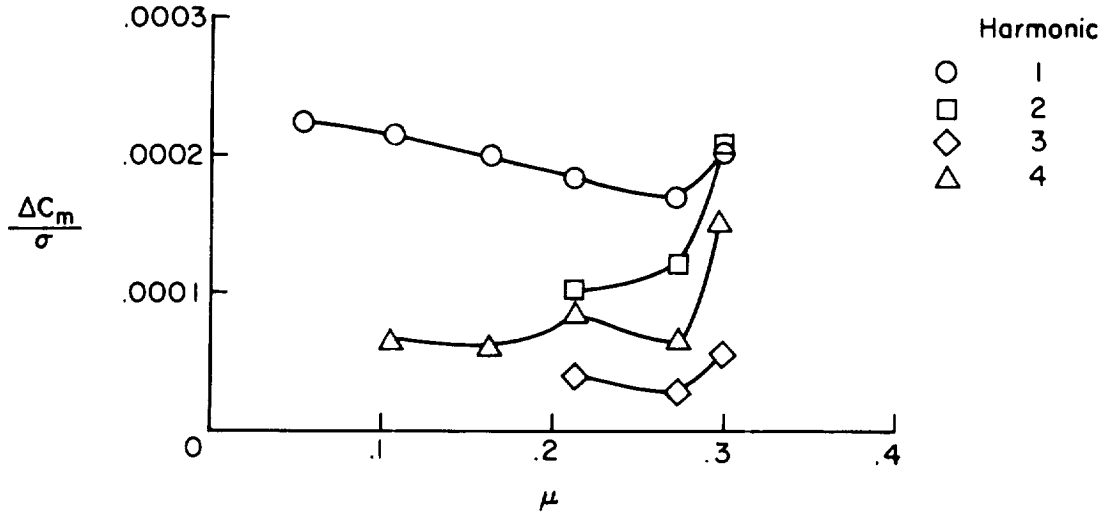

(a) Four-blade rotor. $\theta = 0^\circ$; $\alpha = -5^\circ$.

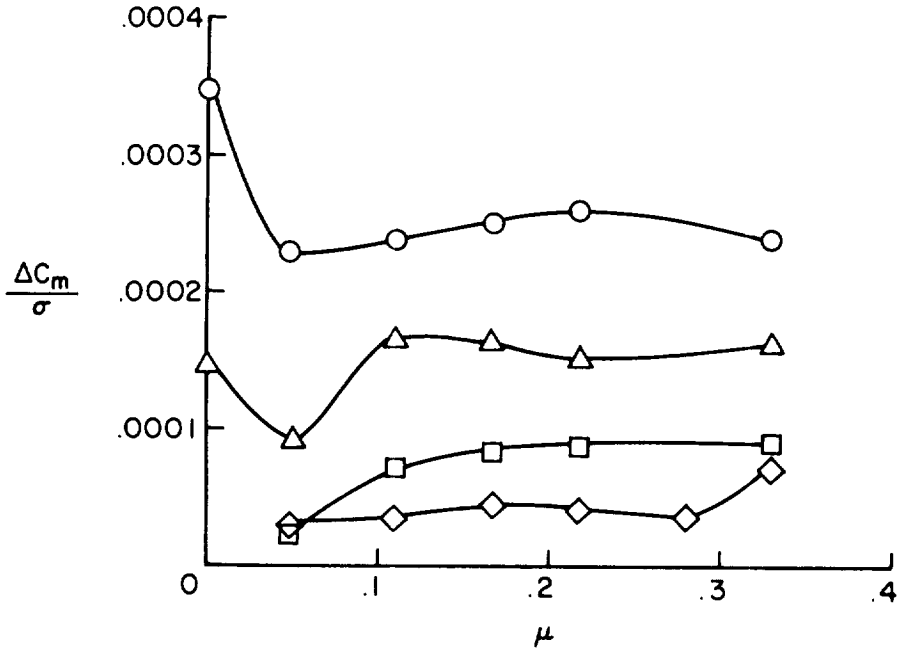

(b) Four-blade rotor. $\theta = 3^\circ$; $\alpha = -5^\circ$.

Figure 17.- Variation of harmonic periodic components of pitching-moment coefficient with tip-speed ratio.

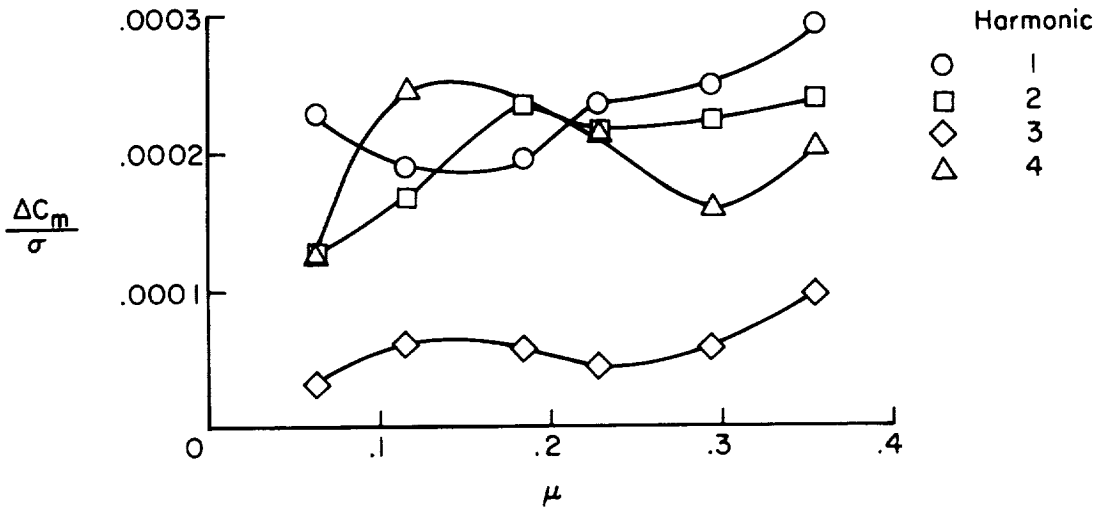

(c) Four-blade rotor. $\theta = 6^{\circ}$; $\alpha = -5^{\circ}$.

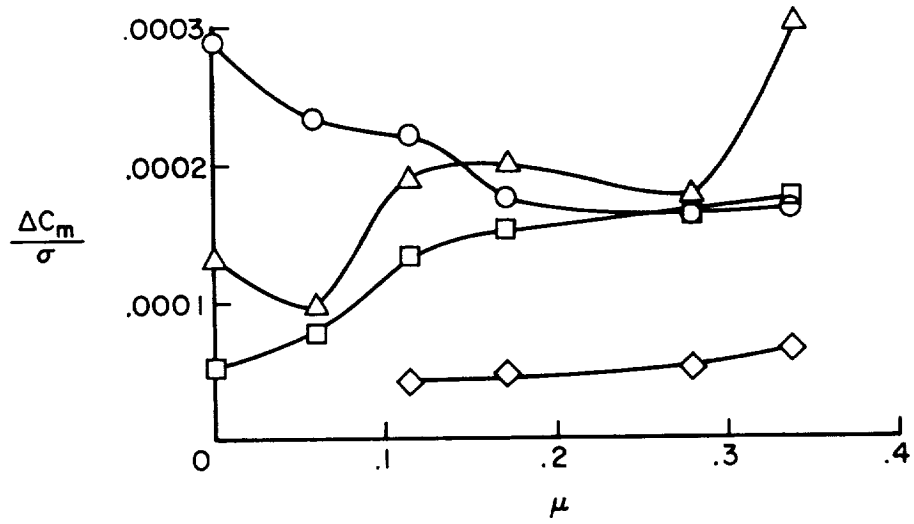

(d) Four-blade rotor. $\theta = 6^{\circ}$; $\alpha = -10^{\circ}$.

Figure 17.- Continued.

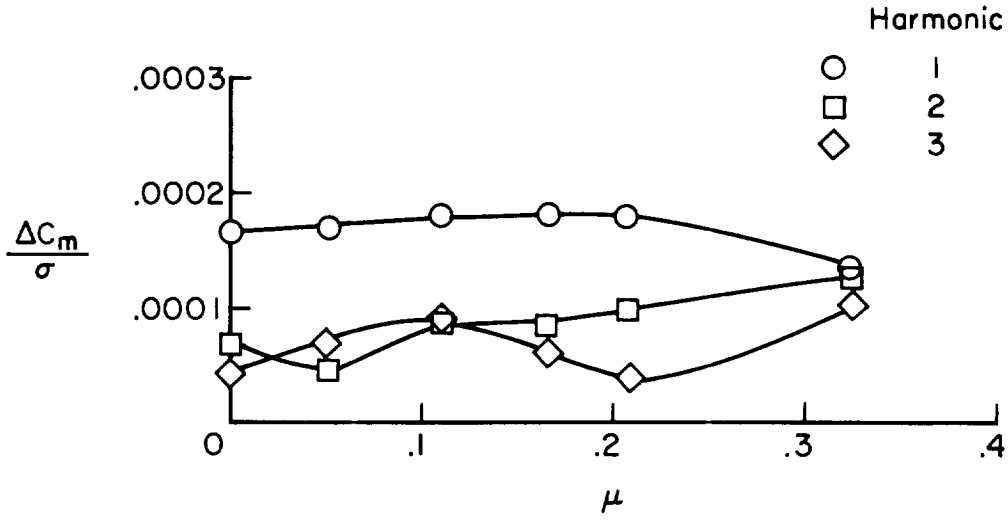

(e) Three-blade rotor. $\theta = 3^\circ$; $\alpha = -5^\circ$.

Figure 17.- Concluded.

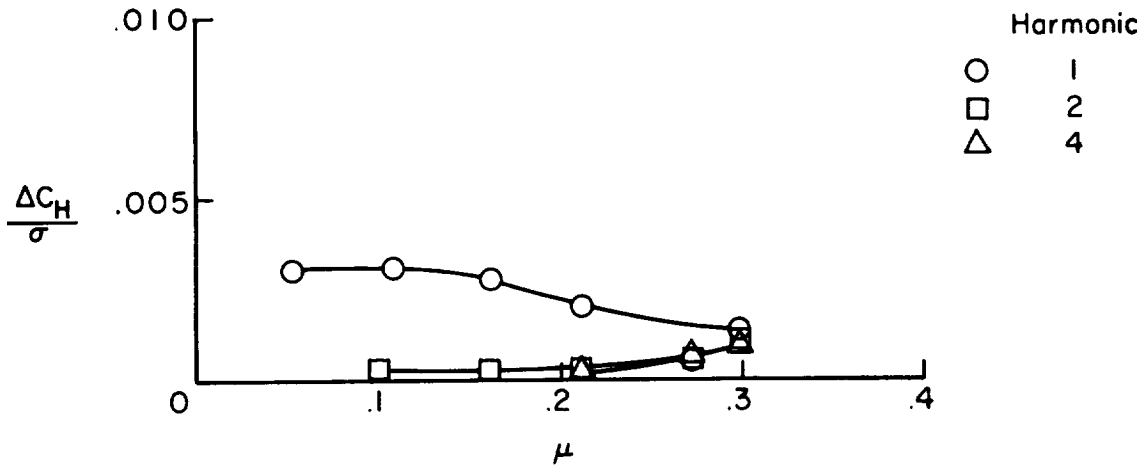

(a) Four-blade rotor. $\theta = 0^\circ$; $\alpha = -5^\circ$.

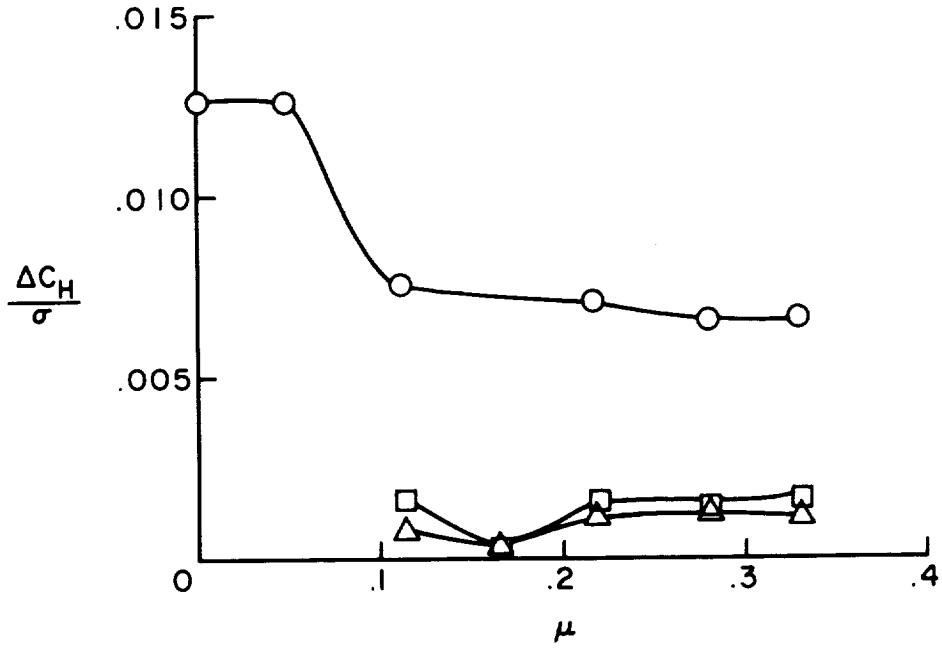

(b) Four-blade rotor. $\theta = 3^\circ$; $\alpha = -5^\circ$.

Figure 18.- Variation of harmonic periodic components of H-force coefficient with tip-speed ratio.

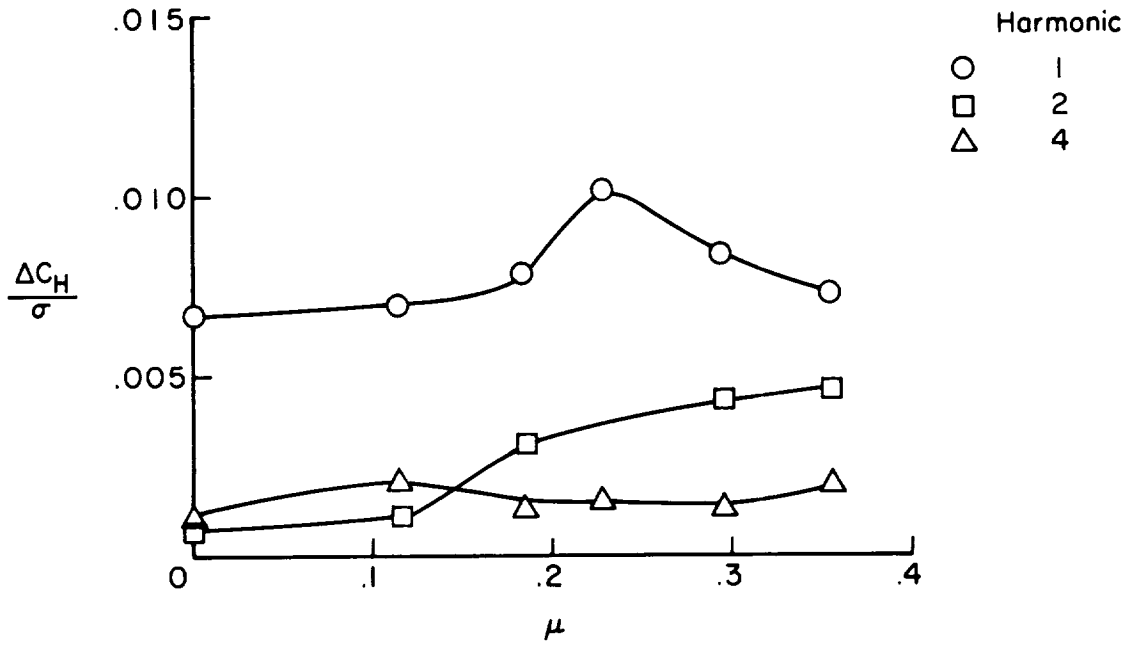

(c) Four-blade rotor. $\theta = 6^\circ$; $\alpha = -5^\circ$.

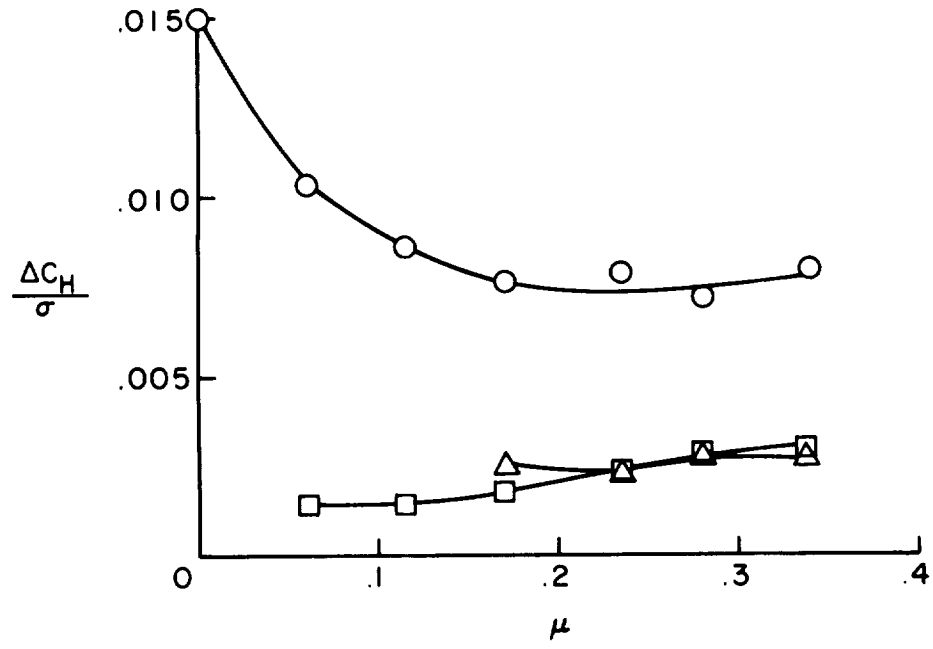

(d) Four-blade rotor. $\theta = 6^\circ$; $\alpha = -10^\circ$.

Figure 18.- Continued.

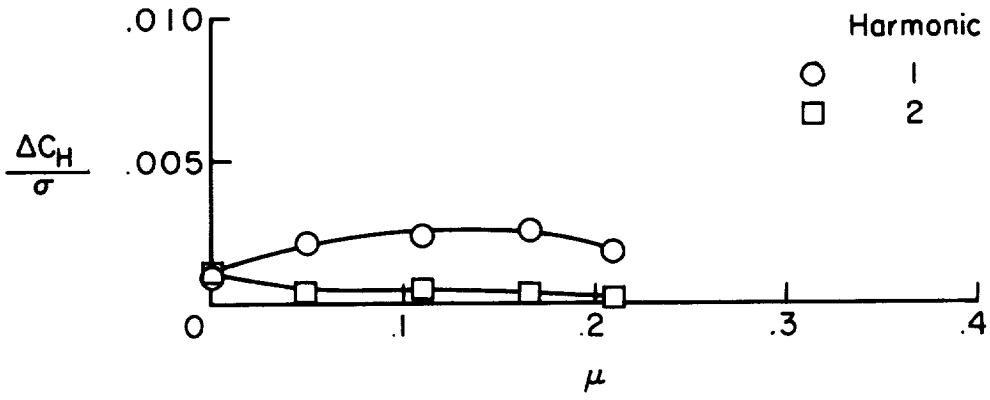

(e) Three-blade rotor. $\theta = 3^\circ$; $\alpha = -5^\circ$.

Figure 18.- Concluded.

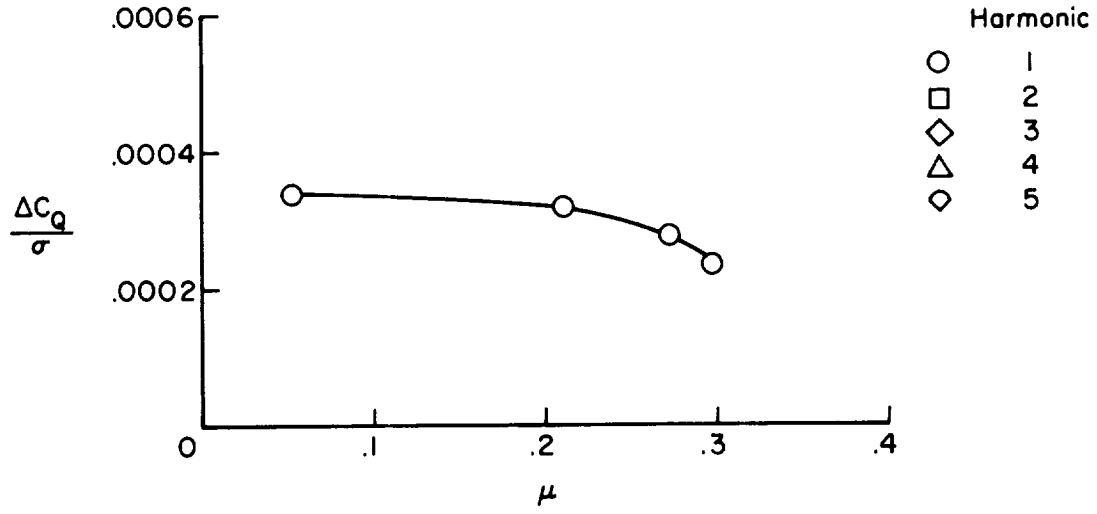

(a) Four-blade rotor. $\theta = 0^\circ$; $\alpha = -5^\circ$.

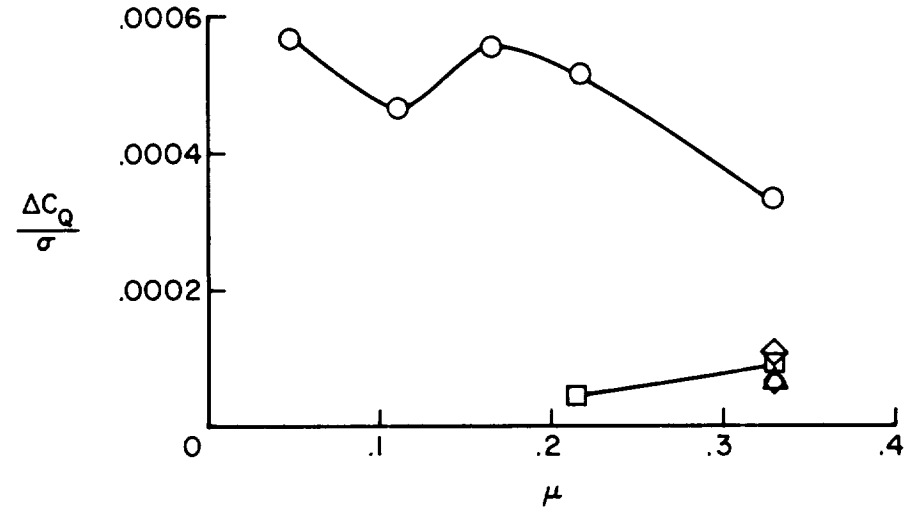

(b) Four-blade rotor. $\theta = 3^\circ$; $\alpha = -5^\circ$.

Figure 19.- Variation of harmonic periodic components of torque coefficient with tip-speed ratio.

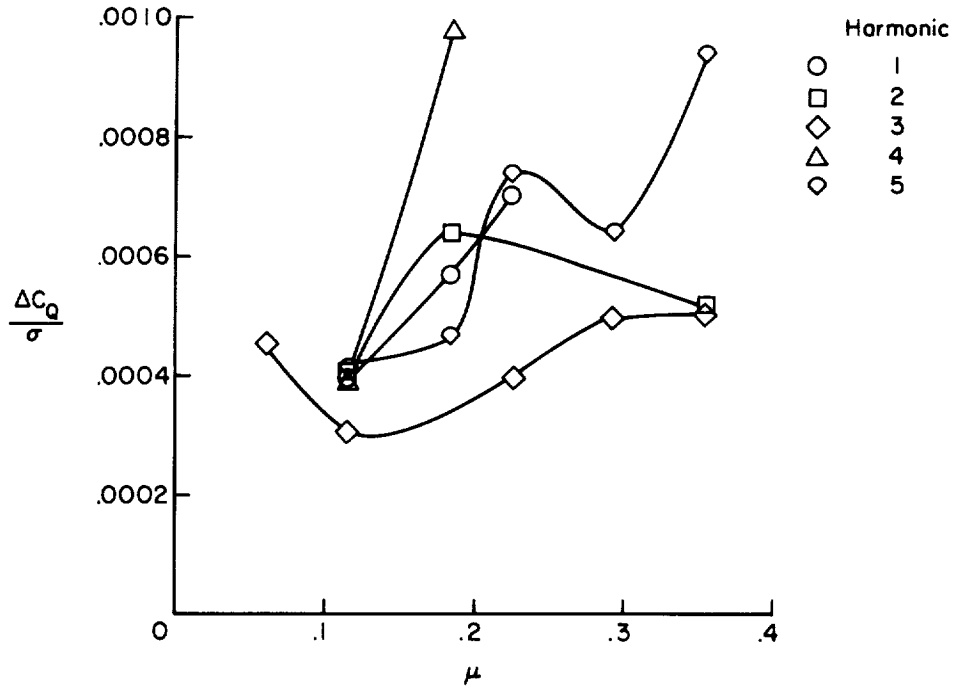

(c) Four-blade rotor. $\theta = 6^\circ$; $\alpha = -5^\circ$.

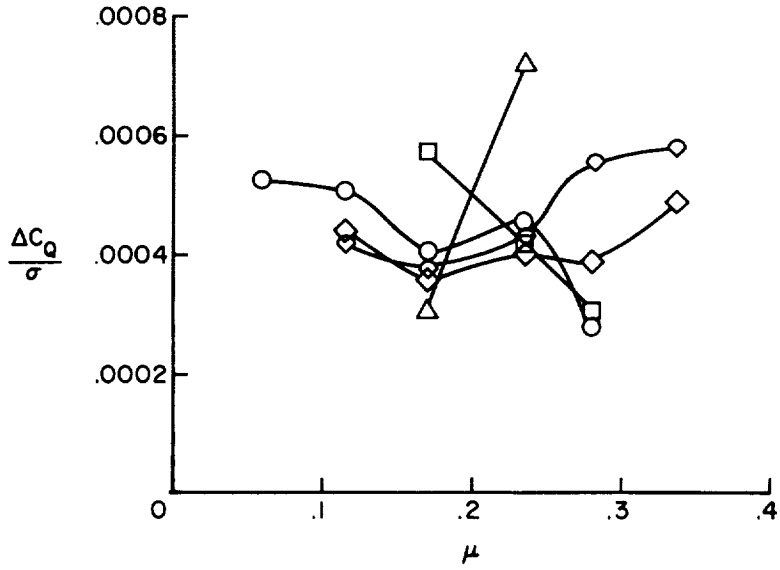

(d) Four-blade rotor. $\theta = 6^\circ$; $\alpha = -10^\circ$.

Figure 19.- Continued.

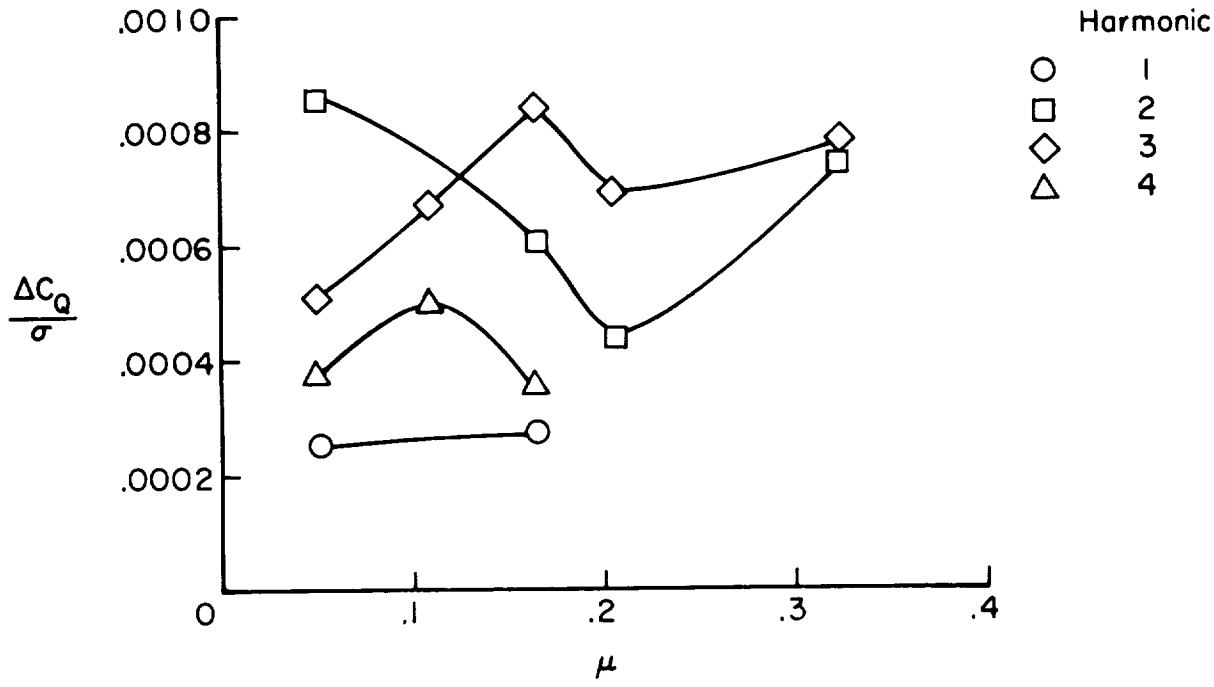

(e) Three-blade rotor. $\theta = 3^\circ$; $\alpha = -5^\circ$.

Figure 19.- Concluded.